Author's Accepted Manuscript

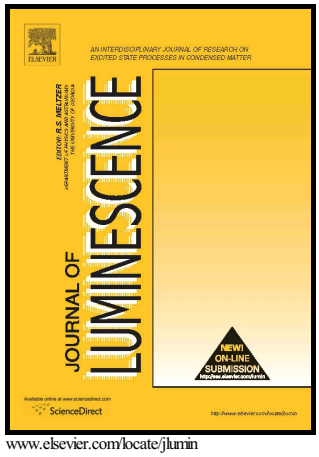

www.elsevier.com/locate/jlumin

Monovalent ions co-doped $SrTiO_3:Pr^{3+}$ nanostructures for visualization of latent fingerprints and as a red component for solid state devices

S. Yeshodamma, D.V. Sunitha, R.B. Basavaraj, G.P. Darshan, B. Daruka Prasad, H. Nagabhushana

PII: S0022-2313(18)31199-2
DOI: https://doi.org/10.1016/j.jlumin.2018.12.044
Reference: LUMIN16173

To appear in: *Journal of Luminescence*

Received date: 3 July 2018
Revised date: 26 November 2018
Accepted date: 19 December 2018

Cite this article as: S. Yeshodamma, D.V. Sunitha, R.B. Basavaraj, G.P. Darshan, B. Daruka Prasad and H. Nagabhushana, Monovalent ions co-doped $SrTiO_3:Pr^{3+}$ nanostructures for visualization of latent fingerprints and as a red component for solid state devices, *Journal of Luminescence,* https://doi.org/10.1016/j.jlumin.2018.12.044

This is a PDF file of an unedited manuscript that has been accepted for publication. As a service to our customers we are providing this early version of the manuscript. The manuscript will undergo copyediting, typesetting, and review of the resulting galley proof before it is published in its final citable form. Please note that during the production process errors may be discovered which could affect the content, and all legal disclaimers that apply to the journal pertain.

ACCEPTED MANUSCRIPT

Monovalent ions co-doped $SrTiO_3:Pr^{3+}$ nanostructures for visualization of latent fingerprints and as a red component for solid state devices

S. Yeshodamma[1], D.V. Sunitha[1,*], R.B. Basavaraj[2], G.P. Darshan[3], B. Daruka Prasad[4,*], H. Nagabhushana[2,*]

[1]School of Applied Sciences (Physics), Reva University, Rukmini Knowledge Park, Kattigenahalli, Yelahanka, Bangalore - 560064 India.
[2]Prof. C.N.R. Rao Centre for Advanced Materials Research, Tumkur University, Tumkur 572 103, India
[3]Department of Physics, Acharya Institute of Graduate Studies, Bangalore 560 107, India
[4]Department of Physics, BMS Institute of Technology and Management, Affiliated to Visveswaraiah Technological University-Belagavi, Bangalore 560 064, India

sunithaprasad8@gmail.com
darukap@bmsit.in
bhushanvlc@gmail.com
*Corresponding Author/s

Accepted manuscript

Abstract

Structural and luminescence properties of $SrTiO_3$: Pr^{3+}: A^+ (A^+: Li, Na, K) nanophosphors were synthesized by simple sonochemical route. Prepared products were well-characterized for their optical and structural properties. Surface morphology of the prepared samples were studied with the influential parameters such as surfactant concentration, sonication time, temperature, pH and compared the effect with normal mechanical stirring. Morphology was highly dependent on the experimental parameters. The predicted growth mechanism to obtain superstructures of the samples prepared by sonochemical method was discussed. Photoluminescence (PL) studies exhibit characteristic emission peaks of Pr^{3+} ions in the range 500-750 nm. The highest PL intensity was obtained for 5 mol% of Pr^{3+} doped samples. Further, co-doping with Li^+, Na^+ and K^+ ion into Pr^{3+} activated $SrTiO_3$ phosphor led to an enhancement in luminescence intensity by reducing the parity restriction of electric dipole transitions. As a consequence of suitable local distortion of the crystal field surrounding to the Pr^{3+} activator ions. The maximum PL intensity was observed for Li^+ (1 wt %) co-doped $SrTiO_3:Pr^{3+}$ (5 mol %) samples. Furthermore, Li^+ ion was the best charge compensator, because of it reduced the defects emission and also increased the emission intensity of Pr^{3+} significantly. Prepared phosphors exhibit short lifetime, good quantum efficiency; excellent color purity which is near to the NTSC standards. Prepared fluorescent powders were used as a dusting powder for the rapid visualization of latent fingerprints under UV light of 254 nm. From the reported results it is evident that the optimized prepared samples are suitable for solid state lighting and advanced forensic investigation applications.

Graphical Abstract:

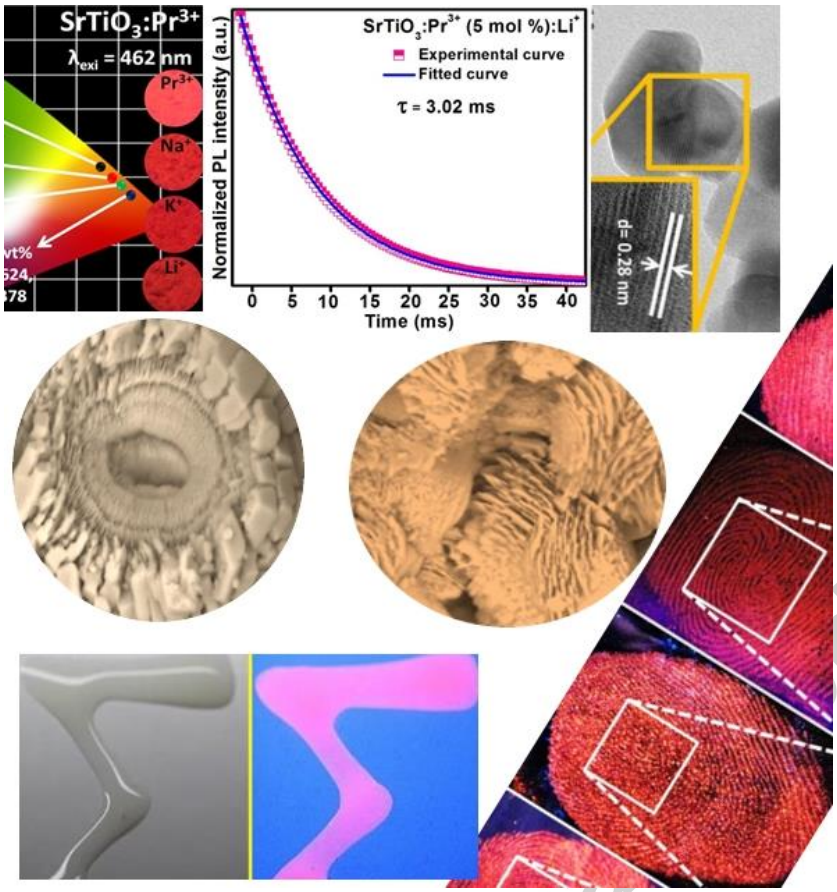

Keywords: - Latent Finger Prints; Forensic Science; Luminescent powder; Display devices; Anti-counterfeiting applications.

1. Introduction

Phosphor materials showed their potentiality in the fields of display devices, white LEDs, and optical devices due to their less energy consumption capability [1, 2]. Recently nanophosphor materials which showed much better solution for these applications. Therefore, there is a lot of scope to fabricate superior luminescent nanophosphors (NPs) having special spectral potentials. Trivalent rare earth (RE) ions doped in a suitable host matrix was a familiar approach to attain outstanding luminescence spectral characteristics. Emission behavior of the RE ions depends on the surrounding environment; choice of host plays an important role in realizing rich luminescence features of the phosphor. This was due to active energy transfer from the host material to dopant ions [3-5]. Strontium titanate ($SrTiO_3$) is considered to be an ideal host due to its wide energy band gap (3.3 eV) and its

Accepted manuscript

ACCEPTED MANUSCRIPT

compositional stability at extreme environmental conditions. This helps $SrTiO_3$ to use for many applications namely; dynamic random access memory, tunable microwave gadgets, photo-electrodes for hydrogen production, hydrogen storage etc. [6-8].

Monovalent, alkali metal ions like Li^+, K^+ and Na^+ have low oxidation state and small ionic radii which can alter the local site symmetry of RE ions doped inside the host matrix. Among these monovalents, Li^+ is used in large due to their role as a flux, supports for the charge trapping and for the creation of oxygen vacancies, high diffusivity of Li^+ ions in the host matrix and easily alters the crystal field [9, 10]. However, to the best of our knowledge the co-doping effect of Na^+ and K^+ monovalent ions in the $SrTiO_3$: Pr^{3+} material matrix is not reported so far.

Fingerprints (FPs) analyses have provided reliable evidence for exact identification of individuals. In the criminal investigations, FPs were considered as major proof due to their tenacity and individuality features. These FPs are mainly grouped into latent, patent, and plastic prints [11, 12]. Among these latent fingerprints (LFPs) were unseen to eyes but they consist of sweat and oil traces of the culprit transferred from the skin surface to the various articles used by offender at the crime scene [13-17]. Hence, a better visualization technique is necessary to make them visible effectively and must be able to preserve for long duration. Small irregularities occur within the friction ridges of the LFPs called as Galton's details are of bifurcation, ridge endings, and dots or islands pattern must be viewed clearly for the precise identification [18-20]. From past few decades, several LFPs visualization techniques have been developed such as powder dusting, vacuum metal deposition, ninhydrin, cyanoacrylate, iodine fuming, fluorescence staining etc. [21, 22]. Among these, powder dusting technique is simple and easy but it has the drawbacks of low visibility, use of toxic powders, blurriness and fast decay [23]. Still visualization of LFPs on dark background colored surfaces and transparent surfaces were quite challenging. To find suitable solution to this RE ions doped luminescent materials are employed for the visualization of LFPs assisting both class and individual ridge characteristics [24-26]. Li^+, K^+ and Na^+ co-doped $SrTiO_3$: Pr^{3+} prepared samples were used as powder dusting and reported their effectiveness in visualization of LFPs. Preparing and using of security ink to protect the counterfeit money and to avoid the forgery of a private documents is one more challenging [27,28]. Prepared samples were also used for testing their potentiality as a security ink to overcome the problem of counterfeiting.

For the preparation of NPs, various synthesis techniques were employed such as solid state reaction, solution combustion, ultrasonication, hydrothermal, solvothermal, sol-gel etc.

Accepted manuscript

ACCEPTED MANUSCRIPT

[29-32]. Among these methods of preparation, ultrasonication method was considered as one of the facile approach. Because of preparation under ambient conditions, able to obtain high homogeneity, easily scalable to industry requirements and low cost [16,33,34]. High temperature and partial pressures with adiabatic nature in the system creates the acoustic cavitation which destroys the attractive forces among the molecules leads to the formation of nanopowders [35-37]. Sonochemistry is the field where the formation, development and crumple of the acoustic cavitation during the reaction was studied. This route is simple, single step approach, able to produce high purity, narrow size distribution and fast reaction rate. Additionally, it brings down the crystallization temperature and because of its rapid synthesis procedure it can be easily scalable to industrial needs [38].

In the present work, structural, morphological and luminescence properties of $SrTiO_3$: Pr^{3+} (1-11 mol %) and $SrTiO_3$: $Pr^{3+}{}_{(5\ mol\%)}$: A^+ (A^+: Li, Na, K) nanophosphors synthesized by sonochemical route using EGCG as a surfactant were reported. Various experimental parameters such as ultrasound irradiation time, surfactant concentration, effect of pH and frequency were changed to study the morphology and luminescence properties of the final product. Superstructures (SS) were obtained in the morphology features was explained through growth mechanisms. Samples were characterized for their structural, morphological and compositional informations. Photoluminescence properties of the samples were explored for their use in various solid state and forensic applications. Prepared samples were effectively used for the visualization of LFPs on various porous and non-porous surfaces. Also checked for the anti-counterfeiting applications of the prepared samples.

Accepted manuscript

2. Experimental

2.1. Synthesis of Monovalent (Li, Na, K) co-doped $SrTiO_3$:Pr^{3+} phosphors

Analytical grade strontium chloride hexahydrate [$SrCl_2$. $6H_2O$, (99.9 %)], Titanium (IV) chloride [$TiCl_4$ (99 %)] and Praseodymium (III) Chloride [$PrCl_3$, (99.9 %)] were procured from Sigma Aldrich and used without further purification. Alkali chlorides, ($LiCl_2$, NaCl and KCl) were used as alkali metal ion sources, which act as a co-dopant in the preparation of $SrTiO_3$: Pr^{3+}. Stoichiometric quantities of the chemicals along with bio-surfactant (Epigallocatechin gallate (EGCG)) were taken in 500 ml beaker and thoroughly mixed using double distilled water. Further, the pH of the precursor solution was adjusted by adding KOH

ACCEPTED MANUSCRIPT

solution of 1M. The resultant precursor solution was subjected to sonication treatment with a titanium horn probe (frequency and power of ~ 20 kHz and 300 W). After the sufficient ultrasound irradiation, the obtained precipitate was thoroughly washed with ethanol and were calcined to ~ 200 °C for 3 h. The schematic illustration for the fabrication of $SrTiO_3$: Pr^{3+} (1-11 mol %) NP by sonochemical route was showed in Fig. 1.

2.2. Visualization of LFPs by using $SrTiO_3$:Pr^{3+} (5 mol %) NPs co-doped with Li^+ (1 wt %) ion

LFPs used in the present study were collected from a healthy single donor. Before impression of the LFPs, the donor hands were cleaned thoroughly and dried in air and deposited the LFPs on various forensic related porous and non-porous surfaces. Highest PL intensity showed NPs were applied carefully by smooth brushing method as a dust for powder dusting method. Developed LFPs were photographed using a digital camera under UV 254 nm light.

2.3 Preparation of $SrTiO_3$:Pr^{3+} (5 mol %): Li^+ (1 wt %) luminescent ink

In order to develop luminescent security ink, $SrTiO_3$:Pr^{3+} (5 mol %): Li^+ (1 wt %) NPs were well dissolved in a standard polyvinyl alcohol (PVA) gold medium using a magnetic stirring followed by ultrasonication for ~ 10 min. The obtained transparent solution was used as luminescent ink by pouring into a dip pen to draw various labels and visualized these drawings under 254 nm light. Fig.2. shows the pictorial representation of the (a) visualization of LFPs under 254 nm UV light using $SrTiO_3$:Pr^{3+} (5 mol %) nanophosphor by powder dusting process. Fig.2(b) shows development process for anti-counterfeiting labels.

2.2. Characterization techniques

Shimadzu 7000- powder x-ray diffractometer with Cuk_α (1.541 Å) radiation was employed for the structural characterization. Hitachi TM-3000 scanning electron microscope (SEM) and H-8100 transmission electron microscope (TEM) were used to study the morphology and to estimate the crystallite size respectively. Photoluminescence (PL) studies were carried out using Jobin Yvon Spectrofluorimeter Fluorolog-3 with Xenon lamp as an excitation source (450 W). The Nikon D3100/AF-S digital camera with 50 mm f/2.8 G ED lens was employed to photograph the developed LFPs under UV 254 nm irradiation light.

3. Results and discussion

3.1 PXRD analysis

Accepted manuscript

ACCEPTED MANUSCRIPT

Fig.3 (a) depicts the powder x-ray diffraction (PXRD) profiles of $SrTiO_3:Pr^{3+}$ (1-11 mol %) NPs. The profiles exhibit single cubic phase with perovskite structure. The obtained results were in good agreement with JCPDS card number 35-0734 [39]. Dopant ions were effectively substituted in $SrTiO_3$ host lattice effectively helps for tuning the optical and electronic properties of these materials. Substitution of Li^+ at Ti^{4+} site is possible if size is only the consideration, but charge difference is quite large and its substitution causes more point defects in crystallites as a consequence, the PL property decreases as compared to $SrTiO_3:Pr^{3+}$ NPs. The average crystallite sizes (D) of the prepared NPs were estimated using Scherrer's relation and Williamson-Hall (W-H) plots (Fig.3c). The 'D' values of the prepared samples were tabulated in Table 1. Fig. 3d shows that there is no major change in the positions of diffraction peaks due to the co-dopant ions except the variation in the x-ray intensity.

3.2. Raman scattering spectral analysis

Room temperature (RT) Raman spectra of the $SrTiO_3:Pr^{3+}$ (5 mol %) co-doped with monovalent (Li^+, Na^+, K^+) NPs are shown in Fig. 4(a). The spectra exhibit peaks at ~ 154, 177, 222, 245, 287, 337, 471, 494, 530, and 640 cm^{-1} in low-energy region, which are owing to the Raman modes of the orthorhombic crystal structure of $SrTiO_3$ [40]. The peaks at ~ 177, 222, 245, 287, and 337 cm^{-1} are assigned to O–Ti–O bending modes. The peaks at ~ 471, 494, and 530 cm^{-1} are related to $Ti–O_3$ torsional modes and the 640 cm^{-1} peak is characteristic of Ti–O symmetric stretching mode. It is interesting to note that when Pr^{3+} was introduced into the $SrTiO_3$ powders, additional new peaks at ~ 798, 1048, 1188, 1371, 1441, 1601, and 1644 cm^{-1} in the high-energy region were observed, which were attributed to localized vibrational modes of the dopant Pr^{3+} ions.

3.3 Fourier Transform Infra-red (FTIR) spectroscopy

To support for the results of section 3.2, Fig. 4(b) shows the FTIR spectra of the synthesized $SrTiO_3:Pr^{3+}$ (5 mol %), M^+ (M^+ = Li, Na and K) NPs. The spectra show absorption bands at 546, 1070, 1442, 1660 and 3461 cm^{-1}. The O-H stretching and bending vibrations of water are related with bands at 3461 and 1660 cm^{-1}. The bands at ~ 1070 and 1442 cm^{-1} were attributed to alcoholic bending vibrations (C-OH functional groups). Broad band between ~ 500 and 800 cm^{-1} were owing to stretching vibrations of $SrTiO_3$ host and Pr^{3+}-O vibrations [41].

ACCEPTED MANUSCRIPT

3.4 Morphological analysis

Scanning electron micrographs of Pr^{3+} doped $SrTiO_3$ NPs prepared by varying ultrasound irradiation time (1-5 h) was shown in Fig.5 (a–f). It was evident from the figure that some irregular aggregates act as a building block for the architectures as observed at 1 h ultrasound irradiation time Fig.5 (a). When the ultrasound irradiation time increased to 2 h, irregular aggregates fragmented and ordered growth. Further, samples fabricated at prolonged ultrasound irradiation times, i.e., 3 and 4 h, individual fragments will undergo self-assembly to form the flat hexagonal disc like structures (Fig. 5 (c & d)). In addition, when ultrasound irradiation time was increased to 5 h, bullets like structures will undergo self- assembly in an oriented direction to form hierarchical flower-like superstructures (Fig. 5 (e, f)).

Fig.6 shows the SEM micrographs of $SrTiO_3$:Pr^{3+} (5 mol %): Li^+ (1 wt %) prepared with various concentrations of bio-surfactant EGCG. When the concentration of EGCG is 5 %W/V, thick edged randomly oriented disc like structures were obtained (Fig.6a). As the concentration of EGCG continues to increase to 10 %W/V the smooth edged disc like structures appears to be fragmented (Fig.6b). Further increase in the EGCG concentration to 15 %W/V these fragmented particles divided into several branches at the edges and stacked together (Fig.6c). However, with further increase in the EGCG concentration to 20-30 %W/V the smooth hexagonal discs are clearly separated from each other (Fig.6 (d-f)). Finally, a flower-like hexagonal structures were formed in the presence of 35 %W/V EGCG concentration (Fig.6g).

The effect of different pH on the morphologies of the product was also studied in detail as shown in Fig.7. When the pH value was set to 1, agglomerated thick edged tumor like structures were obtained (Fig.7a). However, when the pH value was set to 3 and 5, agglomerated tumor like structures undergo self-assembly and form thick edged smooth hexagonal. Further, with increase of pH to 7 and 9, more self-assembled hexagonal structures were appeared (Fig.7 (d-f)). The effect of ultrasonication power on the morphology was shown in Fig.8. It can be observed from the figure that when the ultrasonication power is 20 kHz, irregular shaped thick edged particles were found to be arranged in a circular fashion (Fig.8a). When the power was increased to 24 and 26 kHz these circularly arranged particles were appearing to be separated from each other (Fig.8 b, c). In addition, SEM micrographs of $SrTiO_3$:Pr^{3+} (5 mol %): Li^+ (1 wt %) prepared without ultrasound (using mechanical

Accepted manuscript

ACCEPTED MANUSCRIPT

stirring) was shown in Fig.9. The images revealing that the samples are composed of many agglomerated particles and no obvious structure was observed.

Fig.10 shows the growth mechanism of $SrTiO_3$: Pr^{3+} (5 mol %): Li^+ (1 wt %) NPs exhibiting flower-like hierarchical structures. In the present work, surfactant EGCG acts as a face-inhibitor for the formation of flower-like hierarchical structures. Irregular shaped primary particles obtained at primary stage were utilized as seeds for anisotropic growth in the subsequent process. The surfactant was absorbed on these primary particles by utilizing minimum energy of the system and van der Waals interactions results into curved and tilted nano plates-like structures. These tiny nano plates undergo self-assembly in an edge-to-edge way by an oriented direction. Hence, the shape of the particles gradually evolved to 3D hierarchical flower-like structures with a concavity on the top.

TEM image of the optimized $SrTiO^3$: Pr^{3+} (5 mol %): Li^+ (1 wt %) NPs were shown Fig.11(a, b). From the figure it was evident that each particle appears to be of hexagonal in shape and average crystallite size is ~ 27 nm which is in correlation with PXRD results. From HRTEM image (inset of Fig.11(a)), interplanar spacing (d) between the adjacent lattice planes was found to be ~0.28 nm for (110) plane. Inset of Fig. 11 (b) shows the selected area electron diffraction (SAED) pattern of the sample shows the regular rings confirms the polycrystalline nature. The elemental compositions of SrTiO3: Pr^{3+} (5 mol %) NPs were shown in Fig.11(c) confirms the presence of Sr, Ti, O and Pr ions in the prepared sample without any additional impurities.

3.5. Photoluminescence (PL) property

Fig.12 (a) shows the PL excitation spectrum of $SriO_3$:Pr^{3+} (5 mol %) NPs under 607 nm emission at RT. The spectrum shows various peaks, among them peak at ~ 442 nm was most intense, which is attributed to $^3H_4 \rightarrow {}^3P_1$ transitions of Pr^{3+} ions. Hence the PL emission spectra of $SrTiO_3$:Pr^{3+} (1-11 mol %) NPs were recorded with excitation wavelength of 442 nm (Fig. 12 (b)). The spectra exhibit emission peaks at ~ 491, 527, 607, 626, 647, 685 and 737 nm were ascribed to the $^3P_0 \rightarrow {}^3H_4$, $^3P_1 \rightarrow {}^3H_5$, $^3P_0 \rightarrow {}^3H_5$, $^3P_0 \rightarrow {}^3H_6$, $^3P_0 \rightarrow {}^3F_2$, $^3P_0 \rightarrow {}^3F_3$ and $^3P_0 \rightarrow {}^3F_4$ transitions of Pr^{3+} ions [42]. It was observed from the figure that position and shape of the spectra were exhibited similar trend but intensity of emission peaks changes with respect to Pr^{3+} concentration. The variation of PL intensity as a function of Pr^{3+} concentration

Accepted manuscript

ACCEPTED MANUSCRIPT

was shown in the inset of Fig.12 (b). The PL intensity increases up to 5 mol % of Pr^{3+} and later diminishes. This diminishing nature of PL intensity was mainly due to concentration quenching phenomena attributed to energy transfer among dopant Pr^{3+} ions.

The luminescent property of the phosphors arises from the complex interaction among host structure, activators, defects and interfaces. For $SrTiO_3$ phosphor the Pr^{3+} ions entered the host lattice and specially substituted for Sr^{2+} ions, which induced the charge imbalance for $SrTiO_3$ phosphor [43,44]. The emission spectra of monovalent ions (Na^+, Li^+ and K^+) co doped $SrTiO_3$:Pr^{3+} (5 mol %) NPs excited under 442 nm was shown in Fig.12c. Similar observed trends with varying intensities, indicating that the dopant Pr^{3+} and co dopants had successfully substituted in the $SrTiO_3$ host lattice. The emission intensity trend in the prepared samples follows the order: $Li^+ > Na^+ > K^+$. This order may be explained based on lithium ion size as it is small enough to fit any crystal site and the incorporation of this will not change the lattice constant however the diffraction peak widths at half maxima were sharpened indicates that co-dopants helped in strain relaxation by generating oxygen vacancies. The obtained results suggested that, the co-dopant Li^+ ions decrease the intrinsic defects and also facilitate the energy transfer from host to charge transfer states. According to Dexter theory [45], the type of interaction is of dipole-dipole as evident from the logarithmic plot of (I/x) and (x) with a slope of −0.85 and intercept (Q) of 7.42 (Fig.12 (d)). The energy level energy level diagram of Pr^{3+} ions in $SrTiO_3$ host was shown in Fig.12 (e). The added monovalent elements work as a scavenger for SrO planar faults, leading to the improved intensity. Complexes formed due to the charge compensation of Pr^{3+} and Sr^{2+} sites by monovalent elements substituted at Ti^{4+}. The increased number of derived sites results in an increase in the energy transfer from $SrTiO_3$. The PL intensity enhanced as the concentration of monovalent elements concentration increase was due to increased crystallinity of the samples, morphological changes in nano/micro scale and also due to charge compensation between Sr /Ti and Pr ions [43].

3.6. Decay studies

Fig. 13 (a-d) shows the PL decay curves of $SrTiO_3$:Pr^{3+} (5 mol %), Na^+, K^+, Li^+ NPs under 442 nm excitation and 607 nm wavelength emission. The double exponential function was utilized to fit the obtained data, as follows [46]:

$$I_t = I_1 \exp(-t/\tau_1) + I_2 \exp(-t/\tau_2) \qquad \text{-------- (1)}$$

Accepted manuscript

ACCEPTED MANUSCRIPT

where I_1, I_2 and τ_1, τ_2; PL intensities and corresponding lifetimes in an excited energy state, respectively. The average lifetime ($\tau_{average}$) of doped ions in the excited energy states was estimated by using following relation [47, 48]:

$$\tau_{average} = \frac{I_1\tau_1^{\,2} + I_2\tau_2^{\,2}}{I_1\tau_1 + I_2\tau_2} \qquad \text{--------- (2)}$$

The average lifetimes ($\tau_{average}$) of the prepared samples were estimated and given in the Fig.13. Average lifetime of Pr^{3+} ions present in various chemical and physical environments of the phosphor is based on non-homogeneity or defect structure or in homogeneous energy transfer process within the Pr^{3+} energy levels. In this case Pr^{3+} ions present at the surface of the phosphor show a swift decay, meanwhile Pr^{3+} core ions exhibit slow decay comparatively to the earlier ions. This is the main reason for the bi-exponential nature of these samples. From Fig.13 it is evident that, decay life times have similar behavior with variation in luminescence intensity with respect to Pr^{3+} and monovalent metal ions concentrations. The doping of monovalent alkali metal ions creates the oxygen vacancies. These oxygen vacancies, can act as sensitizers, and may facilitate the efficient energy transfer between the Sr-O and Pr-O, might be the reason for the longer life time values of the alkali metal ions co-doped phosphors compared to non-co-doped phosphors.

The Commission International De- I-Eclairage (CIE) 1931 chromaticity co-ordinates [49 – 52] for $SrTiO_3:Pr^{3+}$ (5 mol %), Na^+, K^+, Li^+ NPs were as shown in Fig.14 (a). It was noticed that the CIE co-ordinates shifted from orange red (0.591, 0.416) to pure red (0.624, 0378) region. This confirms that the optimized $SrTiO_3:Pr^{3+}$ (5 mol %), Li^+ NPs emits pure red emission with high color purity. The emission intensity of Li^+ co-doped samples is 5 times more than that of $SrTiO_3:Pr^{3+}$ (5 mol %) phosphors and has high color purity CIE chromaticity coordinates located at (0.66, 0.34), which is just at the NTSC system standard for red chromaticity. Hence, the phosphor could be excited by not only near-UV but also blue LED in solid-state lighting technology [53].

Corresponding correlated color temperature (CCT) was estimated using standard transformation equations [54, 55]. The CCT diagram of $SrTiO_3:Pr^{3+}$ (5 mol %), Na^+, K^+, Li^+ NPs was given in Fig.14 (b). The average CCT values of the prepared samples were found to be ~1802 K. The obtained values were well acceptable range and quite useful in home appliances. Further, the color purity of the prepared powders was calculated by utilizing the equation [56, 57]:

$$\text{Colour purity} = \frac{\sqrt{(x_s - x_i)^2 + (y_s - y_i)^2}}{\sqrt{(x_d - x_i)^2 + (y_d - y_i)^2}} \qquad \text{---------- (3)}$$

Accepted manuscript

ACCEPTED MANUSCRIPT

where (x_s, y_s) ; the coordinates of a sample point (x_d, y_d) ; the coordinates of the dominant wavelength and (x_i, y_i) ; the co-ordinates corresponds to the highest illumination points. Table 2 gives the color purity values of the obtained samples. From the Table.2 it is noticed that the highest color purity (85 %) was found for Li^+ co-doped samples. Further, quantum efficiency (QE) of the $SrTiO_3$:Pr^{3+} (5 mol %) with monovalent ions (Na^+, K^+, Li^+) co-doped NPs were estimated using the relation [58]:

$$QE = \frac{\text{Number of photons emitted}}{\text{Number of photons absorbed}} = \frac{E_c - E_a}{L_a - L_c} \quad \text{---------- (4)}$$

where, E_C ; the integrated luminescence of the phosphor caused by direct excitation, E_a ; the integrated luminescence from the empty integrating sphere (blank, without sample), L_a; the integrated excitation profile from the empty integrating sphere, L_c; the integrated excitation profile when the sample is directly excited by the incident beam. In the present case, the estimated average QE value was found to be ~ 73 %. The obtained results indicate that the prepared phosphor can be used as a potential candidate for display device applications.

3.7. LFPs observation using $SrTiO_3$:Pr^{3+} (5 mol %), Li^+ NPs as a powder dust.

In order to achieve the sensitivity and selectivity of LFPs, LFPs were stained by prepared NPs via powder dusting method and snapped under 254 nm UV light. Fig.15 (a-e) shows the LFPs visualized with various monovalent metal ions (Na^+, K^+, Li^+) on aluminum foil surface. It was observed from the figure that, the detailed ridge characteristics with high intensity were observed in Li^+ ion blended samples.

To confirm the practical applicability of optimized $SrTiO_3$: Pr^{3+} (5 mol %): Li^+ (1 wt %) NPs for LFPs visualization, a series of experiments were performed on various non-porous surfaces namely, ceramic tile, metal scale, stamp pad, stapler, granite, marble and table spoon (Fig.16 (a-g)). Well defined FPs with three level details were clearly revealed on all surfaces, indicating that optimized sample quite effective for the visualization of LFPs without any background hindrance. Therefore, optimized phosphors can be great potential application for visualization LFPs [59].

To achieve high contrast, enhancing the signal and lowering the background noise were the two approaches. $SrTiO_3$: Pr^{3+} (5 mol %): Li^+ (1 wt %) when used for fingermark development on non-substrates (paper cup, plastic sheet and aluminum foil surface (Fig.18 a-

Accepted manuscript

c) indicated that the substrate surface didn't affect the interaction between optimized NPs with the FPs. As shown in Fig.18 (a), the level 1 detail (whorl ridge pattern) and more comprehensive details of level 2 (bi-furcation, ridge end, island, hook, eye, specialty, bridge, small ridge etc.) could be easily recognized by naked eyes. Furthermore, the level 3 information (sweat pores and scar) can be also obtained, which was highly desired for individual identification. These excellent optical behaviors not only were sufficient for individualization but can also be used for exclusion, which were crucial for forensic investigations by circumventing issues related to sufficient contrast between the background and FP ridges arising from multicolored surfaces. Take the fluorescent images under UV wavelength, for example, the ridge pattern details of LFPs on aluminum foil surface could be clearly identified by bare eyes, which would provide sufficient evidence for individual identification.

The pixel profile of the images at higher resolution indicated both the raised ridges and the furrows were stained using optimized NPs (Fig. 18(b)). The ridges of this developed FPs appeared to be fuzzy, showing the low selectivity. By using optimized NPs as fluorescent labels, the FPs exhibited sharp and well-defined papillary ridges, almost without any background stains. The results revealed that the optimized NPs were present on the ridges rather than in furrows. Furthermore, it was also worth mentioning that our method was so quick, efficient and completed within 30 s after moderate training. Therefore, these results confirmed that the optimized NPs were a potential and valuable candidate for the powder dusting method for visualization of LFPs on various substrates.

Fig.19 shows the visualization of LFPs types of various donors using optimized powders on aluminum foil surface under 254 nm UV light. The LFPs stained by $SrTiO_3$: Pr^{3+} (5 mol %): Li^+ (1 wt %) NPs and commercial powders (TiO_2 and Fe_2O_3) on aluminum foil surface under 254 nm UV light were shown Fig. 18. It concludes that the finger print ridges were not clearly identifying the minutiae ridges in the finger prints stained by conventional powders. However, the synthesized product was noticeably enhanced minutiae ridges effortlessly due to their smaller crystalline size. Hence, it was confirmed that, preparation of nanophosphor was quite useful in order to enhance LFPs in different porous and non-porous materials compared commercial powders (Fig.20). Since the NPs were prepared using EGCG as surfactant, we able to obtain superstructures which have the various kinds of surfaces such as flakes, flower like and diamond like structures. Among these, the optimized one which was considered for the FPs visualization was $SrTiO_3$:Pr^{3+} (5 mol%) and monovalents of 1 wt % each. For these samples, when prepared by ultrasonication method

Accepted manuscript

ACCEPTED MANUSCRIPT

along with the EGCG surfactant, there is a formation of superstructures (Figures. 5 - 8) with high surface to volume ratio and more active surface leading to quantum confinement effects. Also we can see the well-connected networks through SEM images makes the prepared samples to stick to the surface of the LFPs and when exposed to light they can emit the fluorescence light of high intensity. The mechanism of superstructures formation was also dealt in Fig. 10 shows the increased surface activity of the samples. This mechanism is due to the egg box model formed from the EGCG polyphenol network where the NPs trapped [59 - 61]. This increased surface activity makes the dusting powder to stick properly to the LFPs and stays for more time also prevent the sweat pores for long duration. From Fig. 12 (a) and (b) for fluorescent labeling, the PL spectra shows the suitability of broad excitation spectrum, narrow emission spectra and longer fluorescence lifetime are the reasons to select this as better dusting powder to visualize LFPs.

3.8. Anti-counterfeiting analysis

The transparent security ink prepared by $SrTiO_3$: Pr^{3+} (5 mol %): Li^+ (1 wt %) NPs in PVA gold medium under the sunlight and UV light (254 nm) was shown in Fig.21. The several images were printed using prepared ink on white paper and visualized under normal and UV 254 nm light to demonstrate the anti-counterfeiting applications. Fig.21 ((A-D) shows the visualization of anti-counterfeiting labels under normal light. Upon excited under 254 nm UV light counterfeiting labels appears to be intense red as shown in Fig.21 (A^1, B^1, C^1, D^1). The above results reveal that optimized NPs have excellent solubility and dispersion in PVA gold medium and can be applied to the security ink as anti-counterfeiting applications.

4. Conclusions

Nano-sized $SrTiO_3$:Pr^{3+}/A^+ (A = Li, Na and K) nanophosphors were synthesized by sonochemical route. Incorporation of alkali metal ions greatly enhanced the luminescence intensity due to the influence of charge compensation of codoped metal ions. In terms of the emission intensity, the best co-doping alkali ion was determined as Li. Furthermore, the emission intensities were gradually enhanced when the radius of A^+ became smaller was due to the difference of ionic radii which would give rise to the diversity of sub-lattice structure around the luminescent center ions. This fundamental work might be important in developing new luminescent devices using the prepared samples for making components of tricolor

Accepted manuscript

ACCEPTED MANUSCRIPT

lamps, light emitting diodes and display devices. The alkali metal ions co-doped $SrTiO_3:Pr^{3+}$ phosphors showed higher lifetime, better quantum efficiency and excellent chromaticity with high color purity. The optimized sample provides a novel platform for visualization of LFPs on various surfaces under 254 nm light. Therefore, the $SrTiO_3:Pr^{3+}$: Li^+ NPs were the promising materials for WLED's. SEM images of the samples prepared by ultrasonication method were compared with the normal mechanical stirring shows the formation of superstructures with the ultrasonication method. All superstructures were well organized with least utilization of energy as the nature prefers. High surface to volume ratio and confinement effects showed the better adherence of these samples on the LFPs and also helps to prevent the level-3 (Sweat pores) information of the LFPs. Based on the above it can be concluded that the prepared samples are suitable as dusting powder for LFPs visualization and also for anti-counterfeiting application.

Accepted manuscript

ACCEPTED MANUSCRIPT

References

[1]. K.N. Venkatachalaiah, H. Nagabhushana, G P. Darshan, R.B. Basavaraj, B. Daruka Prasad, Novel and highly efficient red luminescent sensor based $SiO_2@Y_2O_3:Eu^{3+}$, M^+ (M^+ = Li, Na, K) composite core–shell fluorescent markers for latent fingerprint recognition, security ink and solid state lightning applications, Sens. Actuators, B 251 (2017) 310-325.

[2]. I. Khan, G. Rooh, R. Rajaramakrishna, N. Sirsittipokakun, H.J. Kim, C. Wongdeeying, J. Kaewkhao, Development of Eu^{3+} doped Li_2O-BaO-GdF_3-SiO_2 oxyfluoride glass for efficient energy transfer from Gd^{3+} to Eu^{3+} in red emission solid state device application, J. Lumin. 203 (2018) 515-524.

[3]. Akanksha Maurya, A. Bahadur, S. B. Rai, Enhanced red emission from Eu^{3+}, A^+ (Li^+, Na^+, K^+) co-doped $CaZrO_3$ phosphor, J. Lumin. 203 (2018) 714-722.

[4]. Renping Cao, Zhihui Shi, Guanjun Quan, Zuofu Hu, Guotai Zheng, Ting Chen, Siling Guo, Hui Ao, Rare-earth free broadband $Ca_3Mg_3P_4O_{16}:Mn^{2+}$ red phosphor: Synthesis and luminescence properties, J. Lumin. 194 (2018) 542-546.

[5]. R.B. Basavaraj, G. P. Darshan, B. Daruka Prasad, S. C. Sharma, H. Nagabhushana, Rapid visualization of latent fingerprints using novel $CaSiO_3:Sm^{3+}$ nanophosphors fabricated via ultrasound route, J. Rare Earths. https://doi.org/10.1016/j.jre.2018.04.019.

[6]. E. A. Mohamed, M. G. Moustafa, I. Kashif, Microstructure, thermal, optical and dielectric properties of new glass nanocomposites of $SrTiO_3$ nanoparticles/clusters in tellurite glass matrix, J. Non-Cryst. Solids. 482 (2018) 223-229.

[7]. Yeqiu Wu, Tao He, Ag loading induced visible light photocatalytic activity for pervoskite $SrTiO_3$ nanofibers, Spectrochim. Acta, Part A. 199 (2018)283-289.

[8]. Agnieszka Lacz, Lukasz Lancucki, Radoslaw Lach, Bartosz Kamecki, Ewa Drozdz, Structural and electrical properties of Cr-doped $SrTiO_3$ porous materials, Int. J. Hydrogen Energy. 43 (2018) 8999-9005.

[9]. A. K. Singh, S.K. Singh, S. B. Rai, Role of Li^+ ion in the luminescence enhancement of lanthanide ions: favorable modifications in host matrices, RSC Adv., 4 (2014) 27039-27061.

[10]. C. Suresh, H. Nagabhushana, G.P. Darshan, R.B. Basavaraj, D. Kavyashree, S.C. Sharma, A. Arulmozhi, B. Daruka Prasad, H.J. Amith Yadav, Facile $LaOF:Sm^{3+}$ based labeling agent and their applications in residue chemistry of latent fingerprint and cheiloscopy under UV visible light, Arabian J. Chem. 11 (2018) 460-482.

[11]. Jin Young Park, Sung Jun Park, Minseok Kwak, Hyun Kyoung Yang, Rapid visualization of latent fingerprints with Eu-doped $La_2Ti_2O_7$, J. Lumin. 201 (2018) 275-283.

[12]. M. Saif, Synthesis of down conversion, high luminescent nano-phosphor materials based on new developed $Ln^{3+}:Y_2Zr_2O_7/SiO_2$ for latent fingerprint application, J. Lumin. 135 (2013) 187–195.

[13]. M Wang, M Li, A. Yu, J Wu, C. Mao, Rare Earth fluorescent nanomaterials for enhanced development of latent fingerprints, ACS Appl. Mater. Interfaces, 7 (2015) 28110-28115.

[14]. T. Kent, Water content of latent fingerprints – Dispelling the myth, Forensic Sci. Int., 266 (2016) 134-138.

[15]. M. Dhanalakshmi, R. B. Basavaraj, G. P. Darshan, S. C. Sharma, H. Nagabhushana, Pivotal role of fluxes in $BaTiO_3:Eu^{3+}$ nano probes for visualization of latent fingerprints on multifaceted substrates and anti-counterfeiting applications, Microchem. J. 145 (2019) 226-234.

Accepted manuscript

ACCEPTED MANUSCRIPT

[16]. Dhanalakshmi Muniswamy, Hanumanthappa Nagabhushana, R.B. Basavaraj, Giriyapura Prabhukumar Darshan, Daruka Prasad B, Surfactant-Assisted $BaTiO_3:Eu^{3+}@SiO_2$ Core–Shell Superstructures Obtained by Ultrasonication Method: Dormant Fingerprint Visualization and Red Component of White Light-Emitting Diode Applications, ACS Sustainable Chem. Eng. 6 (2018) 5214–5226.

[17]. A. Sandhyarani, M.K. Kokila, G.P. Darshan, R.B. Basavaraj, B. Daruka Prasad, S.C. Sharma, T.K.S. Lakshmi, H. Nagabhushana, Versatile core-shell $SiO_2@SrTiO_3:Eu^{3+}$, Li^+ nanopowders as fluorescent label for the visualization of latent fingerprints and anti-counterfeiting applications, Chem. Eng. J. 327 (2017) 1135-1150.

[18]. D. Navami, R. B. Basavaraj, S. C. Sharma, B. Daruka Prasad, H. Nagabhushana, Rapid identification of latent fingerprints, security ink and WLED applications of $CaZrO_3:Eu^{3+}$ fluorescent labelling agent fabricated via bio-template assisted combustion route, Journal of Alloys and Compounds, J. Alloys Compd. 762 (2018) 763-779.

[19]. Kaushal N, Kaushal P, Human Identification and Fingerprints: A Review. J Biomet Biostat., 2 (2011) 123-128.

[20]. R.B. Basavaraj, H. Nagabhushana, G.P. Darshan, B. Daruka Prasad, M. Rahul, S.C. Sharma, R. Sudaramani, K.V. Archana, Red and green emitting CTAB assisted $CdSiO_3:Tb^{3+}/Eu^{3+}$ nanopowders as fluorescent labeling agents used in forensic and display applications, Dyes Pigm. 147 (2017) 364-377.

[21]. R. K. Garg, H. Kumari, R. Kaur, A new technique for visualization of latent fingerprints on various surfaces using powder from turmeric: A rhizomatous herbaceous plant (Curcuma longa), Egypt. J. Forensic Sci., 1 (2011) 53-57.

[22]. G.P. Darshan, H.B. Premkumar, H. Nagabhushana, S.C. Sharma, B. Daruka Prasad, S.C. Prashantha, R.B. Basavaraj, Superstructures of doped yttrium aluminates for luminescent and advanced forensic investigations, J Alloys Compd. 686 (2016) 577 – 587.

[23]. M. Wang, M. Li, M. Yang, X. Zhang, A. Yu, Y. Zhu, P. Qiu, C. Mao, NIR-induced highly sensitive detection of latent fingermarks by $NaYF_4$: Yb, Er upconversion nanoparticles in a dry powder state, Nano Res. 8 (2015) 1800–1810.

[24]. N.H. Deepthi, G.P. Darshan, R.B. Basavaraj, B. Daruka Prasad, H. Nagabhushana, Large-scale controlled bio-inspired fabrication of 3D $CeO_2:Eu^{3+}$ hierarchical structures for evaluation of highly sensitive visualization of latent fingerprints, Sens. Actuators, B. 255 (2018) 3127-3147.

[25]. Benjamin Errington, Glen Lawson, Simon W. Lewis, Gregory D. Smith, Micronised Egyptian blue pigment: A novel near-infrared luminescent fingerprint dusting powder, Dyes Pigm. 132 (2016) 310-315.

[26]. D. R. Taikar, Synthesis and luminescence property of SrY_2O_4:M (M = Eu^{3+}, Tb^{3+}, Sm^{3+}, Ce^{3+}, Bi^{3+}) phosphors, J. Lumin. 204 (2018) 24-29.

[27]. P. Kumar, J. Dwivedi, B. K. Gupta, Highly luminescent dual mode rare-earth nanorod assisted multi-stage excitable security ink for anti-counterfeiting applications, J. Mater. Chem. C 2 (2014) 10468-1075.

[28]. Siyi Dai, Wentao Zhanga, Dongsheng Zhou, Guilin Yan, Sutian Liu, Effect of A^+ (A = Li, Na and K) co-doping on the luminescence enhancement of $CaSr_2(PO_4)_2:Dy^{3+}$ phosphors for white light-emitting diodes, Ceram. Int. 43 (2017) 15493–15499.

[29]. Huajing Gao, Hua Yang, Shifa Wang, Hydrothermal synthesis, growth mechanism, optical properties and photocatalytic activity of cubic $SrTiO_3$ particles for the degradation of cationic and anionic dyes, Optik, 175 (2018) 237-249.

Accepted manuscript

ACCEPTED MANUSCRIPT

[30]. Hiroyuki Ishikawa, Kouya Oohira, Tatsuo Nakajima, Tomohiro Akiyama, Combustion synthesis of $SrTiO_3$ using different raw materials, J. Alloys Compd. 454 (2008) 384-388.

[31]. Jing Xu, Yuelin Wei, Yunfang Huang, Jing Wang, Xuanqing Zheng, Zhixian Sun, Leqing Fan, Jihuai Wu, Solvothermal synthesis nitrogen doped $SrTiO_3$ with high visible light photocatalytic activity, Ceram. Int. 40 (2014) 10583-10591.

[32]. Junhao Zhang, Man Huang, Kazumichi Yanagisawa, Shanshan Yao, NaCl–H2O-assisted preparation of $SrTiO_3$ nanoparticles by solid state reaction at low temperature, Ceram. Int. 41 (2015) 5439-5444.

[33]. Y. Tong, E. Bladt, M. F. Ayguler, A. Manzi, K.Z. Milowska, V. A. Hintermayr, P. Docampo, S. Bals, A.S. Urban, L. Polavarapu, J. Feldmann, Highly luminescent cesium lead halide perovskite nanocrystals with tunable composition and thickness by ultrasonication, Angew. Chem. Int. Ed., 55(2016) 13887-13892.

[34]. R. B. Basavaraj, H. Nagabhushana, B. Daruka Prasad, G. R. Vijayakumar, Zinc silicates with tunable morphology by surfactant assisted sonochemical route suitable for NUV excitable white light emitting diodes, Ultrason. Sonochem. 34 (2017) 700-712.

[35]. D. G. Shchukin, E. Skorb, V. Belova, H. Mohwald, Ultrasonic cavitation at solid surfaces, Adv., Mater., 23 (2011) 1922-1934.

[36]. D. G. Shchukin, H. Mohwald, Sonochemical nanosynthesis at the engineered interface of a cavitation microbubble, Phys. Chem. Chem. Phys., 8 (2006) 3496-3506.

[37]. R.B. Basavaraj, H. Nagabhushana, G.P. Darshan, B. Daruka Prasad, S.C. Sharma, K.N. Venkatachalaiah, Ultrasound assisted rare earth doped Wollastonite nanopowders: Labeling agent for imaging eccrine latent fingerprints and cheiloscopy applications, J. Ind. Eng. Chem. 51 (2017) 90-105.

[38]. M. Dhanalakshmi, H. Nagabhushana, G. P. Darshan, B. Daruka Prasad, Ultrasound assisted sonochemically engineered effective red luminescent labeling agent for high resolution visualization of latent fingerprints, Mater. Res. Bull. 98 (2018) 250-264.

[39]. W. Wang, C. Jiang, M. Shen, L. Fang, F. Zheng, X. Wu, J. Shen, Effect of oxygen vacancies on the red emission of SrTiO3:Pr3+ phosphor films, Appl. Phys. Lett. 94 (2009) 081904, 3 pages.

[40]. Mengjie Qin, Feng Gao, Jakub Cizek, Shengjie Yang, Xiaoli Fan, Lili Zhao, Jie Xu, Gaogao Dong, Mike Reece, Haixue Yan, Point defect structure of La-doped $SrTiO_3$ ceramics with colossal permittivity, Acta Mater. 164 (2019) 76-89.

[41]. Y.L. Du, G. Chen, M.S. Zhang, Investigation of structural phase transition in polycrystalline $SrTiO_3$ thin films by Raman spectroscopy, Solid State Commun. 130 (2004) 577-580.

[42]. X. He, W. Dong, F. Zheng, L. Fang, M. Shen, Effect of tartaric acid on the microstructure and photoluminescence of $SrTiO_3:Pr^{3+}$ phosphors prepared by a sol-gel method, Mater Chem Phys, 123 (2010) 284-288.

[43]. L. Tian, S. Mho, Enhanced luminescence of $SrTiO_3:Pr^{3+}$ by incorporation of Li^+ ion, Solid State Commun., 125 (2003) 647-651.

[44]. D. Guo, X. Zhang, J. Yun, Preparation of compensation ions codoped SrTiO3:Pr3+ red phosphor with the sol-gel method and study of its luminescence enhancement mechanism, Adv Optoelectron., 674780 (2014) 9 pages. http://dx.doi.org/10.1155/2014/674780

[45]. D. L. Dexter, A theory of sensitized Luminescence in solids, J. Chem. Phys. 21 (1953) 836-850.

[46]. H. Ryu, B. K. Singh, K. S. Bartwal, M. G. Brik, I.V. Kityk, Novel efficient phosphors on the base of Mg and Zn Co-doped $SrTiO_3:Pr^{3+}$, Acta Materialia, 56 (2008) 358-363.

Accepted manuscript

ACCEPTED MANUSCRIPT

[47]. W. Tang, Y. Sun, M. Yu, X. Liu, Y. Yin, B. Yang, L. Zheng, F. Qin, Z. Zhang, W. Cao, White light emitting properties of SrTiO3:Pr3+ nanoparticles, RSC Adv 35 (2015) 27491-27495.

[48]. M. Venkataravanappa, H. Nagabhushana, B. Daruka Prasad, G.P. Darshan, R.B. Basavaraj, G.R. Vijayakumar, Dual color emitting Eu doped strontium orthosilicate phosphors synthesized by bio-template assisted ultrasound for solid state lightning and display applications, Ultrason. Sonochem. 34 (2017) 803-820.

[49]. M.D. Fairchild, The CIE 1931 standard colorimetric observer: Mandatory retirement at age 65, Color Res and Appl., 18 (1993) 129-134.

[50]. F. Femila Komahal, H. Nagabhushana, R.B. Basavaraj, G.P. Darshan, B. Daruka Prasad, S.C. Sharma, D. Kavyashree, Design of Bi-functional composite core–shell SiO_2@$ZnAl_2O_4$:Eu^{3+} array as a fluorescent sensors for selective and sensitive latent fingerprints visualization protocol, Adv. Powder Technol. 29 (2018) 1991-2002.

[51]. R. B. Basavaraj, H. Nagabhushana, B. Daruka Prasad, S. C. Sharma, K. N. Venkatachalaiah, Mimosa pudica mediated praseodymium substituted calcium silicate nanostructures for white LED application, J. Alloys Compd. 690 (2017) 730-740.

[52]. C. Suresh, H. Nagabhushana, G.P. Darshan, R.B. Basavaraj, S.C. Sharma, D.V. Sunitha, B. Daruka Prasad, J.F. Williamsh, K. Hareesh, Positron annihilation spectroscopy and photoluminescence investigation of LaOF:Tb^{3+} nanophosphor fabricated via ultrasound assisted sonochemical route, Mater. Sci. Eng., B. 224 (2017) 28-39.

[53]. C.R. Ronda, T. Justel, H. Nikol, Rare earth phosphors: fundamentals and applications, J. Alloys and compd., 275-277 (1998) 669-676.

[54]. J. Schanda, A combined colour preference-colour rendering index, Light Res Technol., 17 (1985) 31-34.

[55]. B.S. Rohini, H. Nagabhushana, G.P. Darshan, R.B. Basavaraj, S.C. Sharma, P. Amudha, M. Rahul, B. Daruka Prasad, Multi-functional applications of self - Assembled 3D CeO_2: Cr^{3+} hierarchical structures synthesized via ultrasound assisted sonochemical route, J. Alloys Compd. 724 (2017) 897-909.

[56]. K.N. Venkatachalaiah, H. Nagabhushana, G.P. Darshan, R.B. Basavaraj, B. Daruka Prasad, S.C. Sharma, Blue light emitting Y_2O_3:Tm^{3+} nanophosphors with tunable morphology obtained by bio-surfactant assisted sonochemical route, Spectrochim. Acta, Part A. 184 (2017) 89-100.

[57]. B. Marappa, M. S. Rudresha, R. B. Basavaraj, G. P. Darshan, B. Daruka Prasad, S. C. Sharma, S. Sivakumari, P. Amudha, H. Nagabhushana, EGCG assisted Y_2O_3:Eu^{3+} nanopowders with 3D micro-architecture assemblies useful for latent finger print recognition and anti-counterfeiting applications, Sen. and Actu. B: Chem. 264 (2018) 426-439.

[58]. H. Nagabhushana, R. B. Basavaraj, B. Daruka Prasad, S. C. Sharma, H. B. Premkumar, Udayabhanu, G R Vijayakumar, Facile EGCG assisted green synthesis of raspberry shaped Cdo Nanoparticles, J. Alloys Compd. 669 (2016) 232-239.

[59]. Zhiming Gao, Y. Fang, Y. Cao, H Liao, K. Nishinari, G. O. Phillips, Hydrocolloid-food component interactions, Food Hydrocolloids, 69 (2017) 149-156.

[60]. X. Michalet, F. Pinaud, T. D. Lacoste, M. Dahan, M. P. Bruchez, A. P. Alivisatos, S. Weiss, Properties of fluorescent semiconductor nanocrystals and their application to biological labeling, Single Mol. 2 (2001) 261-276.

[61]. C. Suresh, H. Nagabhushana, R.B. Basavaraj, G.P. Darshan, D. Kavyashree, B. Daruka Prasad, S.C. Sharma, R. Vanithamani, SiO_2@LaOF:Eu^{3+} core-shell functional nanomaterials for sensitive visualization of latent fingerprints and WLED applications, J. Colloid Interface Sci. 518 (2018) 200-215.

Accepted manuscript

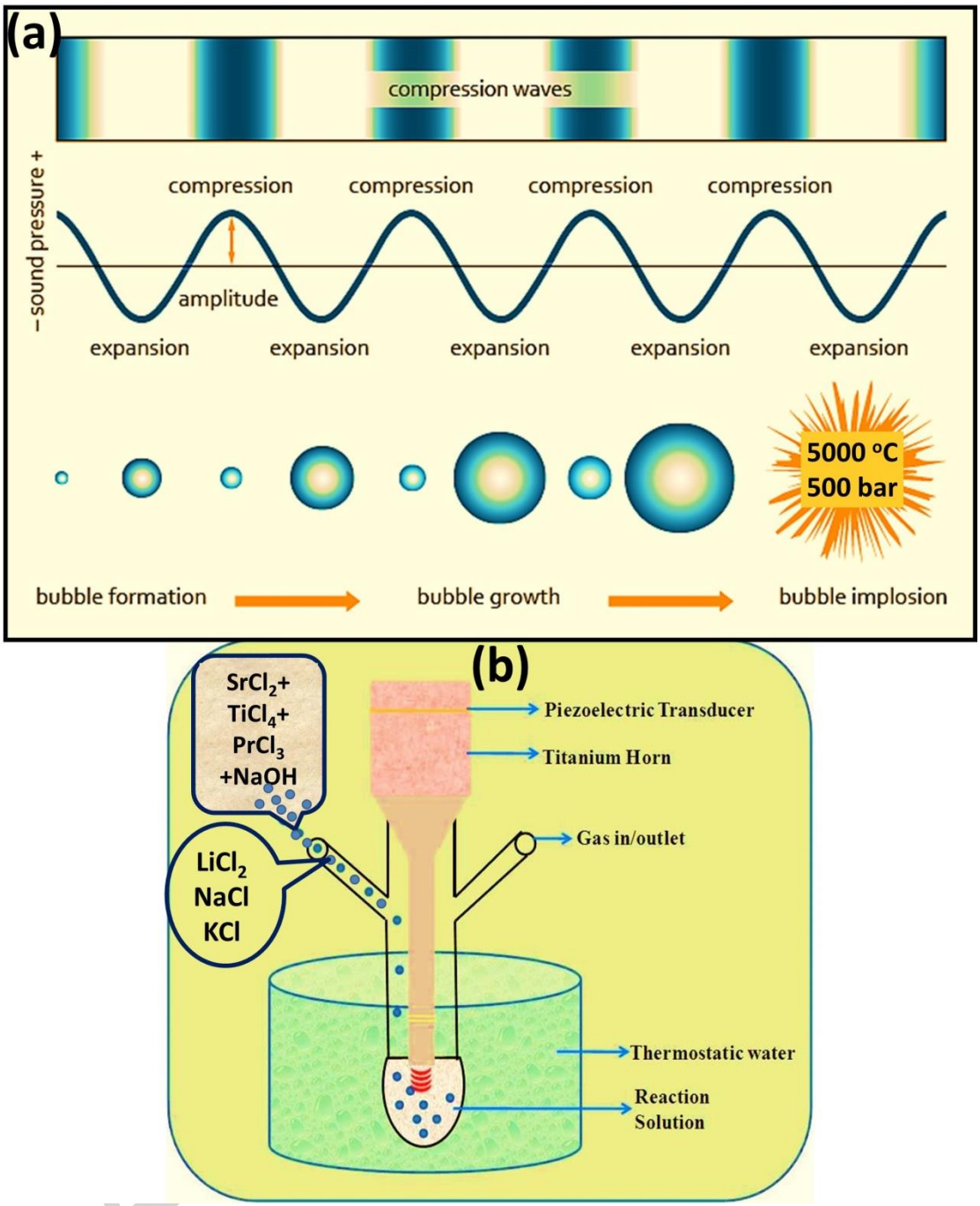

Fig.1. (a) Steps involved in the sonochemical process and (b) schematic diagram for the synthesis of $SrTiO_3$:Pr^{3+} (1-11 mol %) and $SrTiO_3$: $Pr^{3+}{}_{(5\ mol\%)}$: A^+ (A^+: Li, Na, K) nanophosphors by ultrasound assisted sonochemical method.

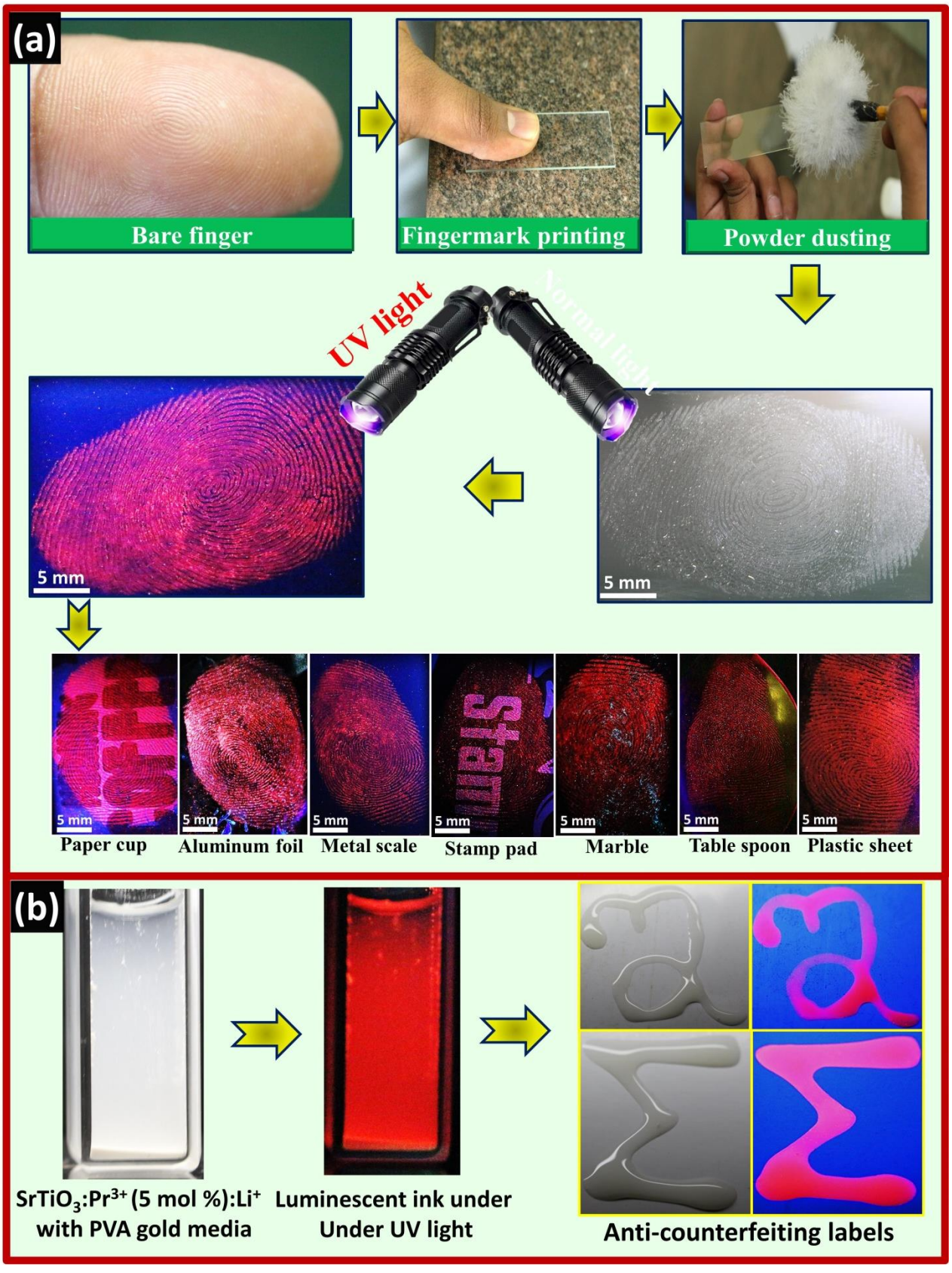

Fig.2.Pictorial representation of the (a) visualization of LFPs under 254 nm UV light using $SrTiO_3:Pr^{3+}$ (5 mol %): Li^+ (1 wt%) nanophosphor by powder dusting process and (b) development process of anti-counterfeiting labels.

ACCEPTED MANUSCRIPT

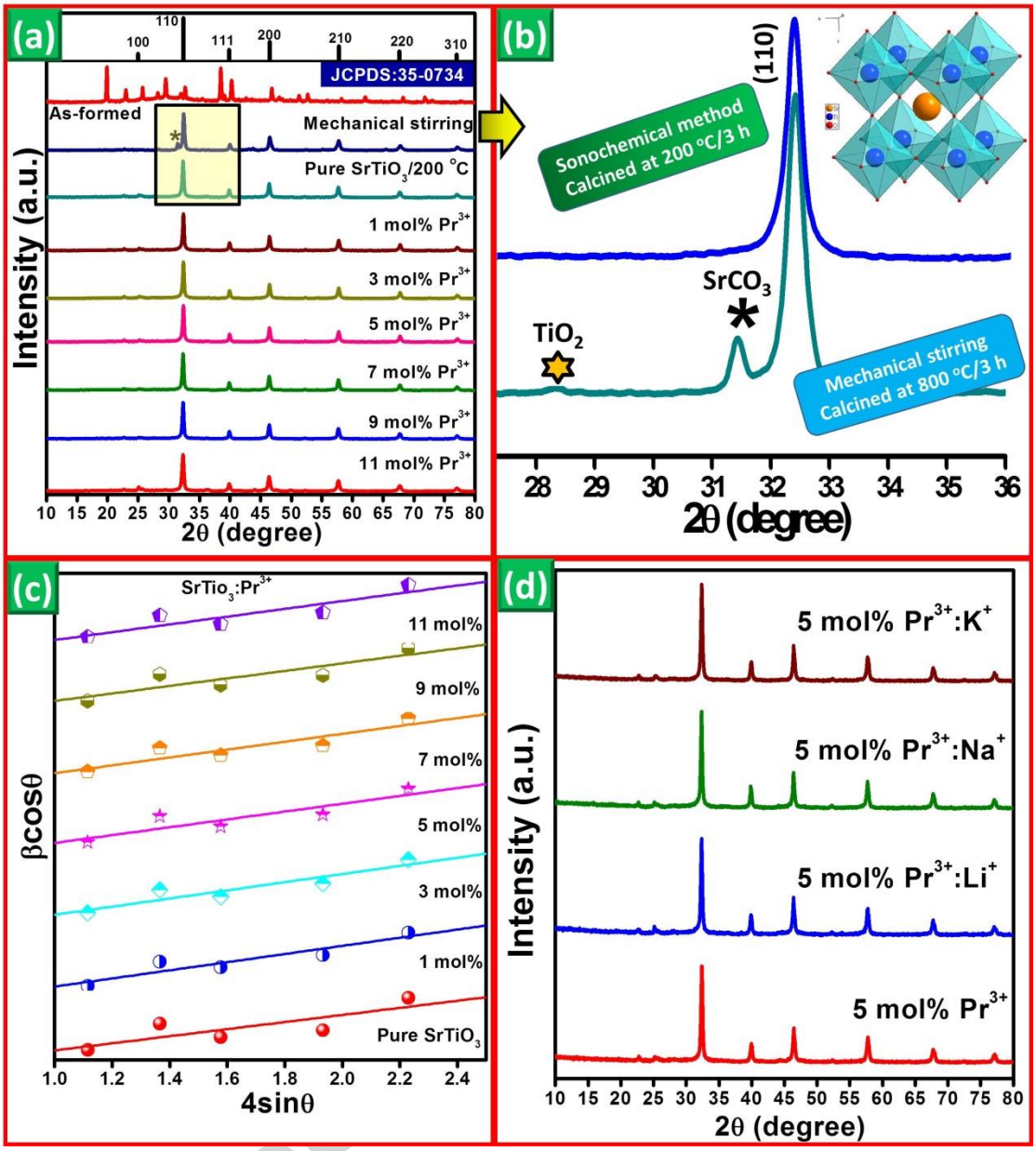

Fig.3 PXRD patterns of (a) $SrTiO_3$: Pr^{3+} (1-11 mol %), (b) Comparison of PXRD patterns of sonochemical and mechanical stirring routes, (c) W-H Plots, (d) $SrTiO_3$: $Pr^{3+}{}_{(5\ mol\%)}$: A^+ (A^+: Li, Na, K) nanophosphors.

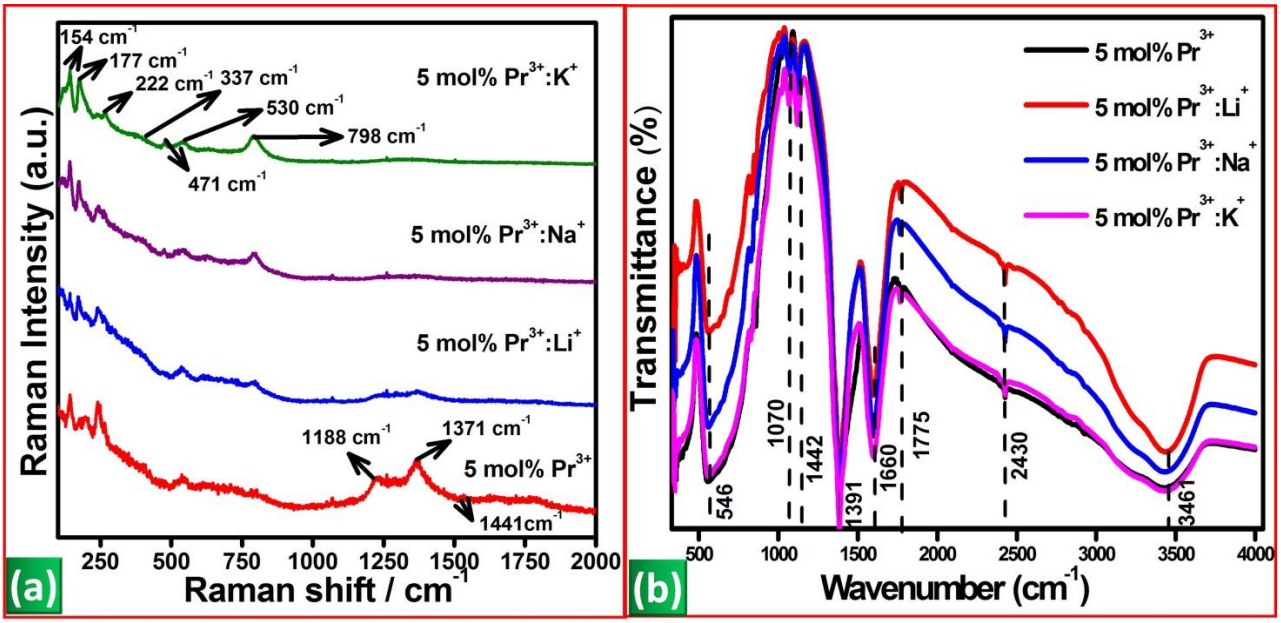

Fig.4 (a) Raman and (b) FTIR Spectra of $SrTiO_3$: Pr^{3+} (1-11 mol %) and $SrTiO_3$: Pr^{3+} $_{(5\ mol\%)}$: A^+ (A^+: Li, Na, K) nanophosphors.

Accepted manuscript

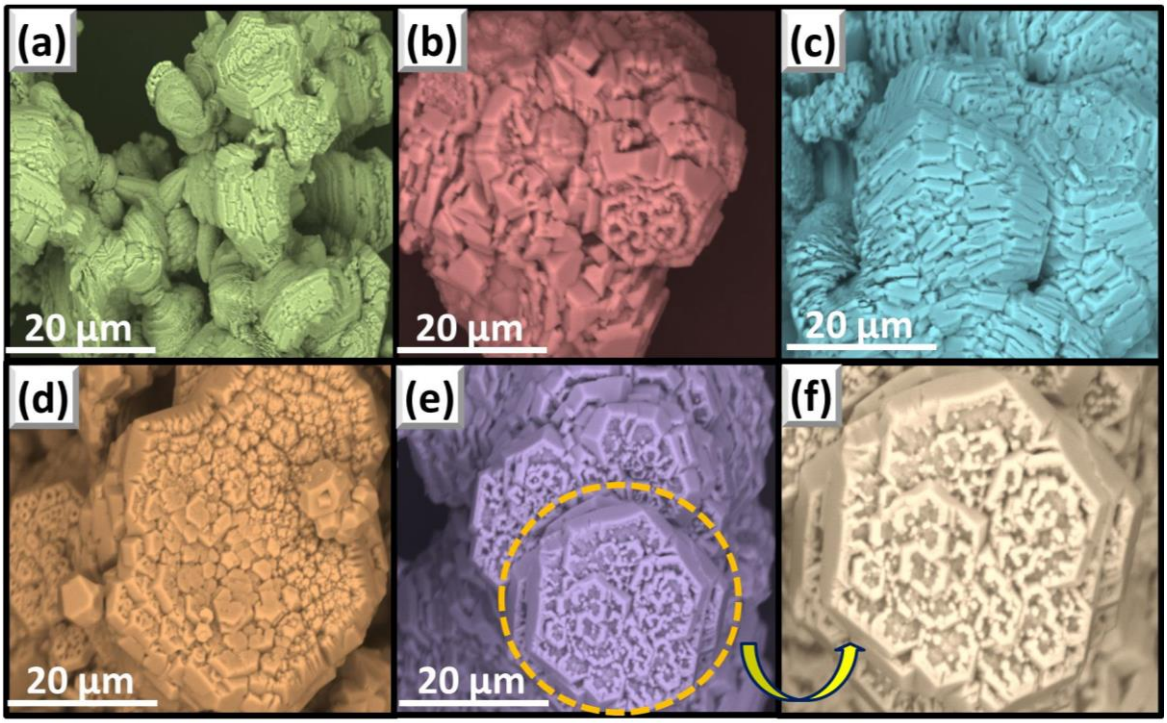

Fig.5 SEM images of Pr^{3+} (5 mol %) doped $SrTiO_3$ NPs prepared by the varying ultrasound irradiation time (a) 1h (b) 2h (c) 3h (d) 4 h (e) 5 h and (f) Zoomed portion of fig. (e).

Accepted manuscript

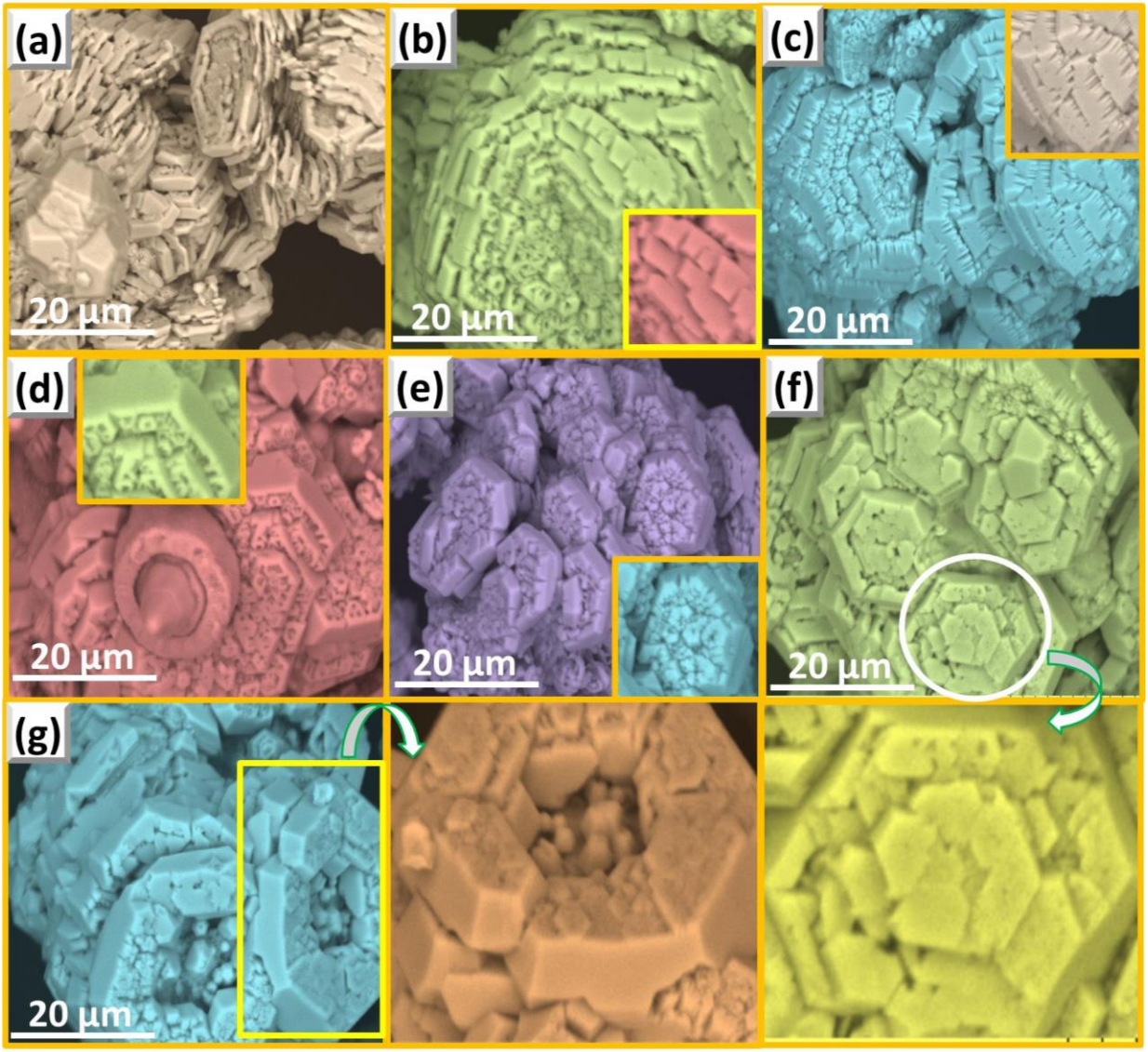

Fig.6 SEM micrographs of $SrTiO_3$:Pr^{3+} (5 mol %): Li^+ (1 wt %) prepared with various concentrations of bio-surfactant EGCG (a) 5 %W/V, (b) 10 %W/V (c) 15 %W/V (d) 20 %W/V (e) 25 %W/V (f) 30 %W/V (g) 35 %W/V.

Accep

ACCEPTED MANUSCRIPT

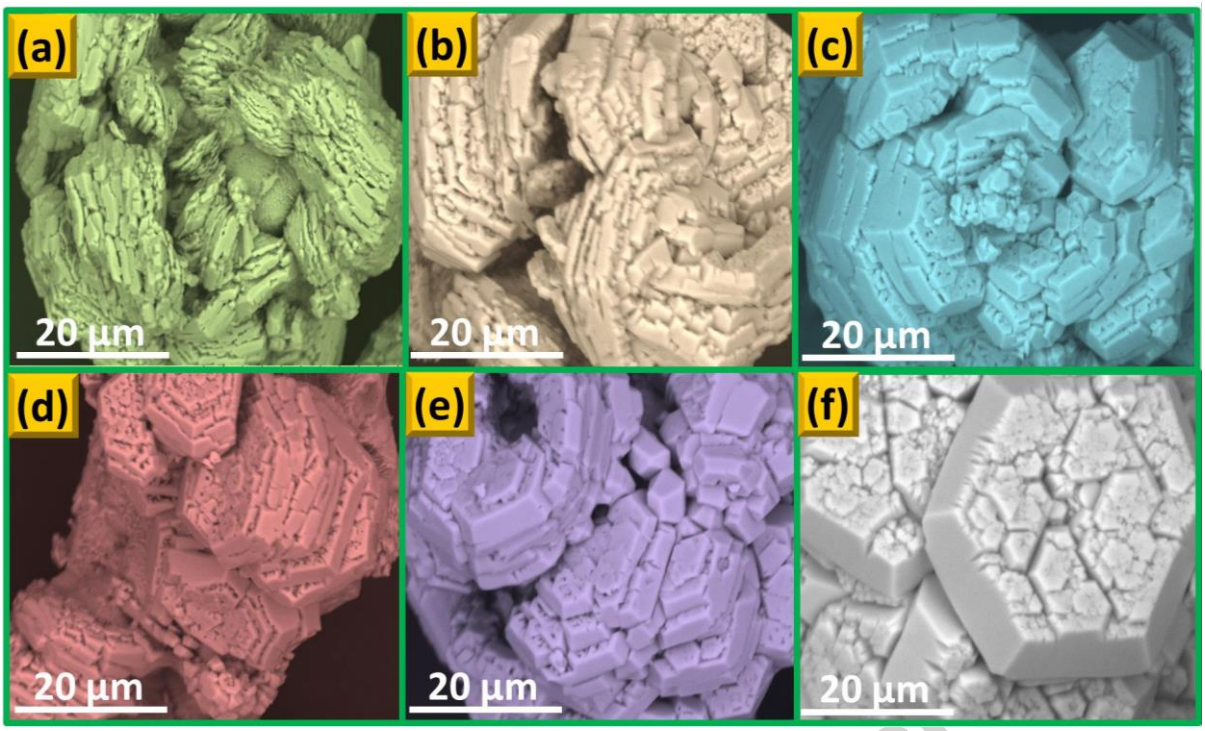

Fig.7. Effect of different pH (a) 1 (b) 3 (c) 5 (d) 7 and (e) 9 on the morphologies of the product.

Accepted manuscript

ACCEPTED MANUSCRIPT

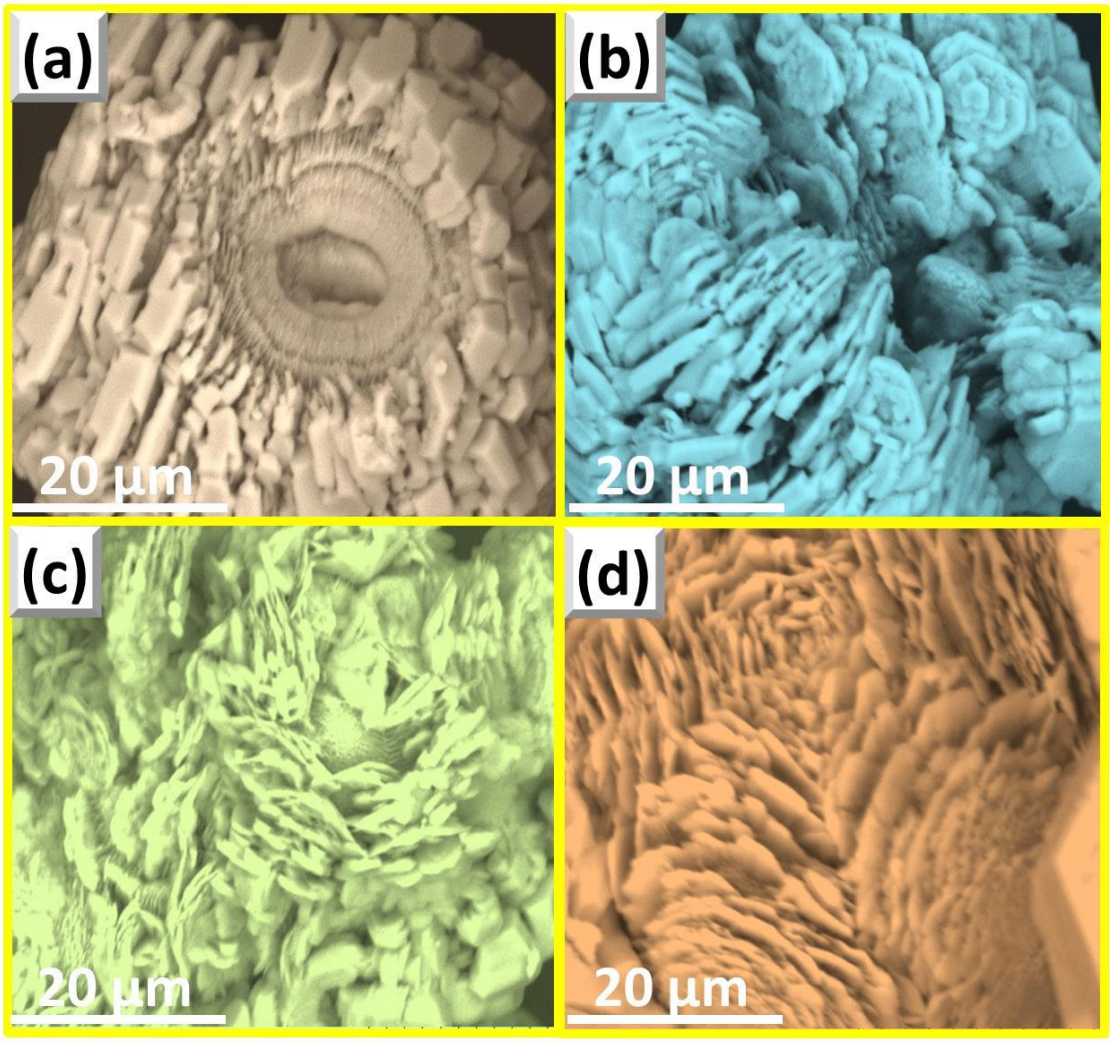

Fig.8 Effect of ultrasonication power on the morphology of the samples (a) 20 kHz (b) 22 kHz (c) 24 kHz and (d) 26 kHz.

Accepted

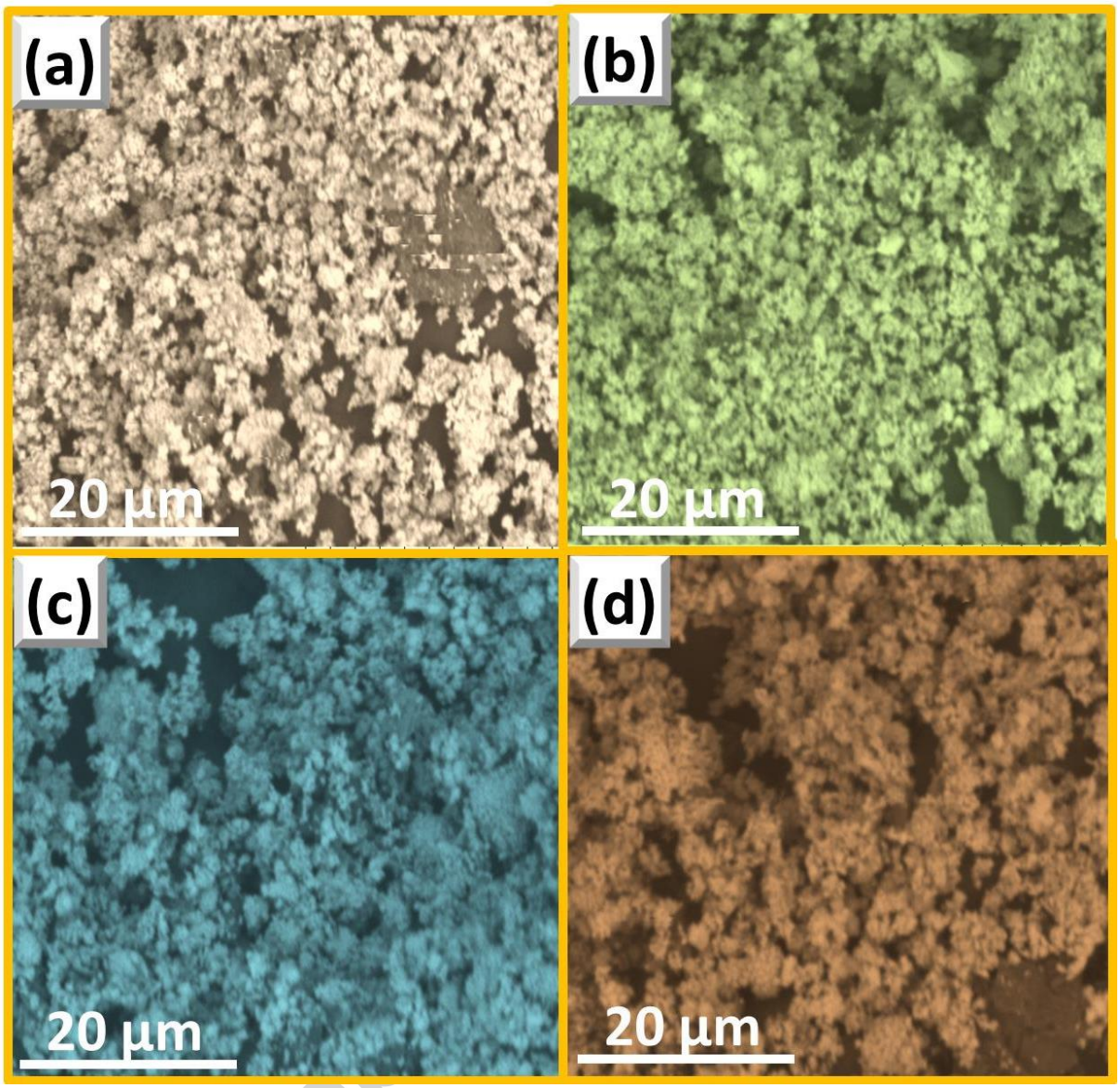

Fig.9 SEM micrographs of $SrTiO_3$:Pr^{3+} (5 mol %): Li^+ (1 wt %) prepared using mechanical stirring method.

Accepted

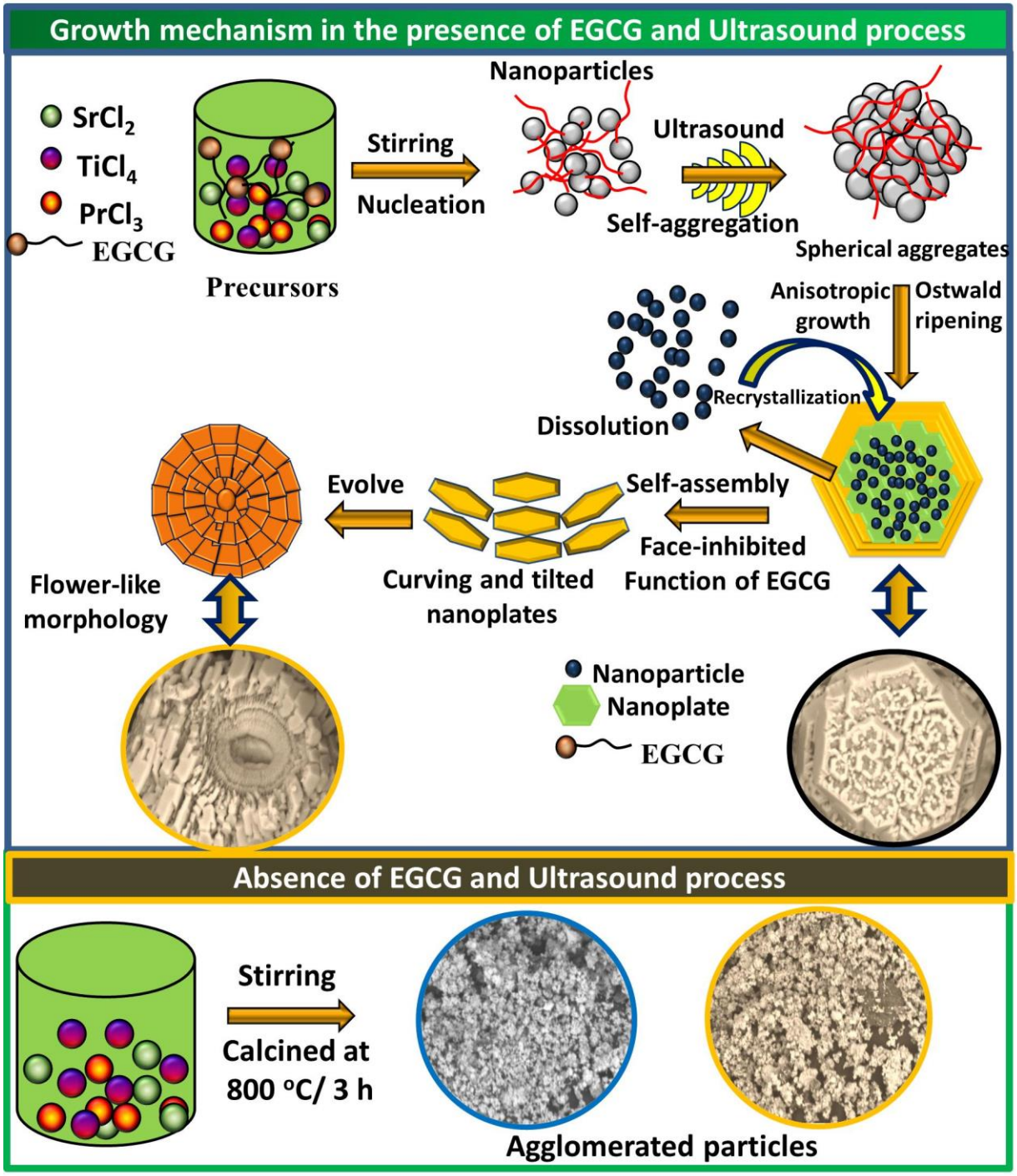

Fig.10 Growth mechanism of $SrTiO_3$: Pr^{3+} (5 mol %): Li^{+} (1 wt %) NPs exhibiting flower-like hierarchical structures with EGCG surfactant.

ACCEPTED MANUSCRIPT

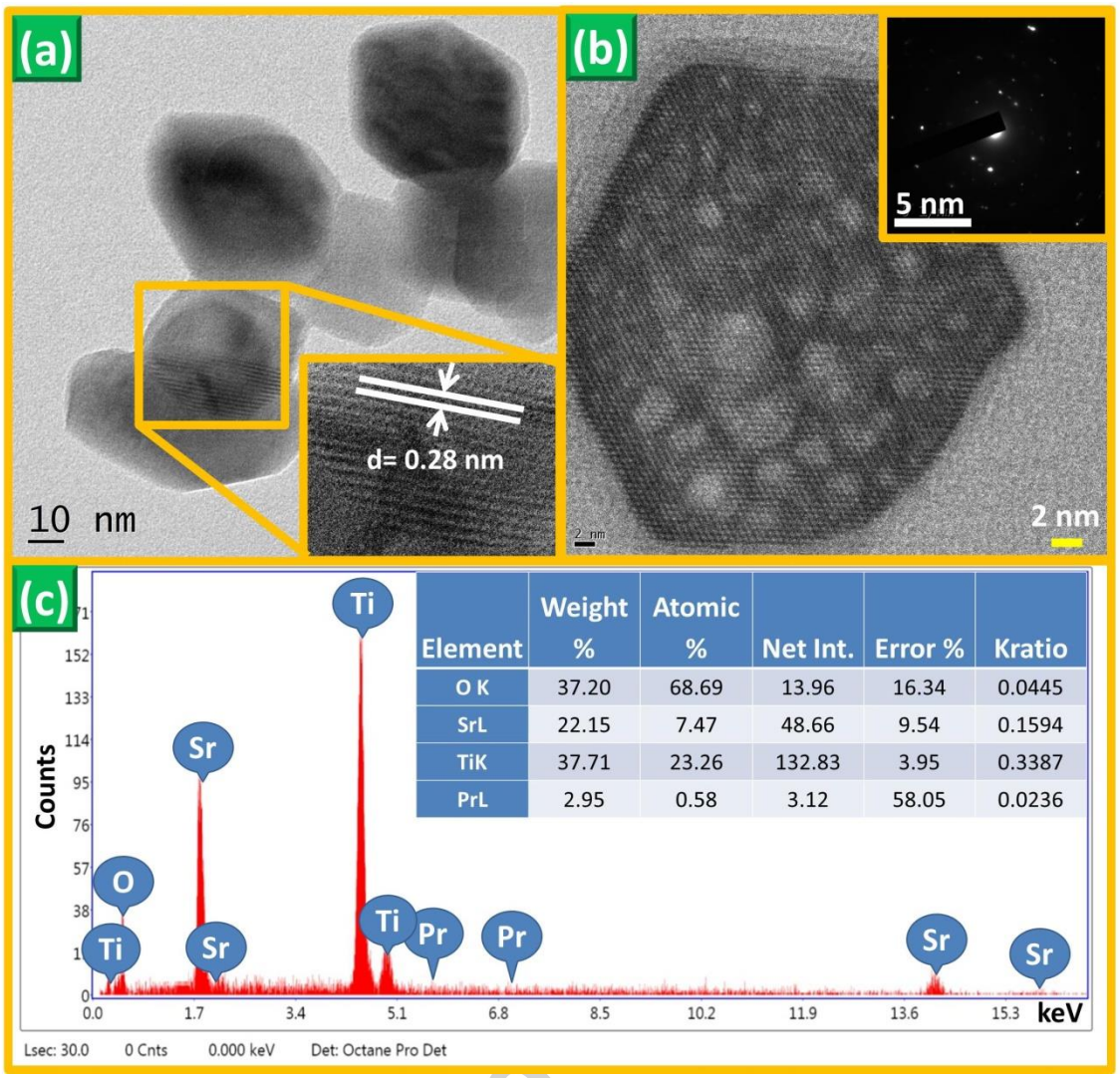

Fig.11 (a) and (b) TEM images of the optimized $SrTiO^{3}$: Pr^{3+} (5 mol %) NPs and (c) Elemental compositions of the sample.

Accepted

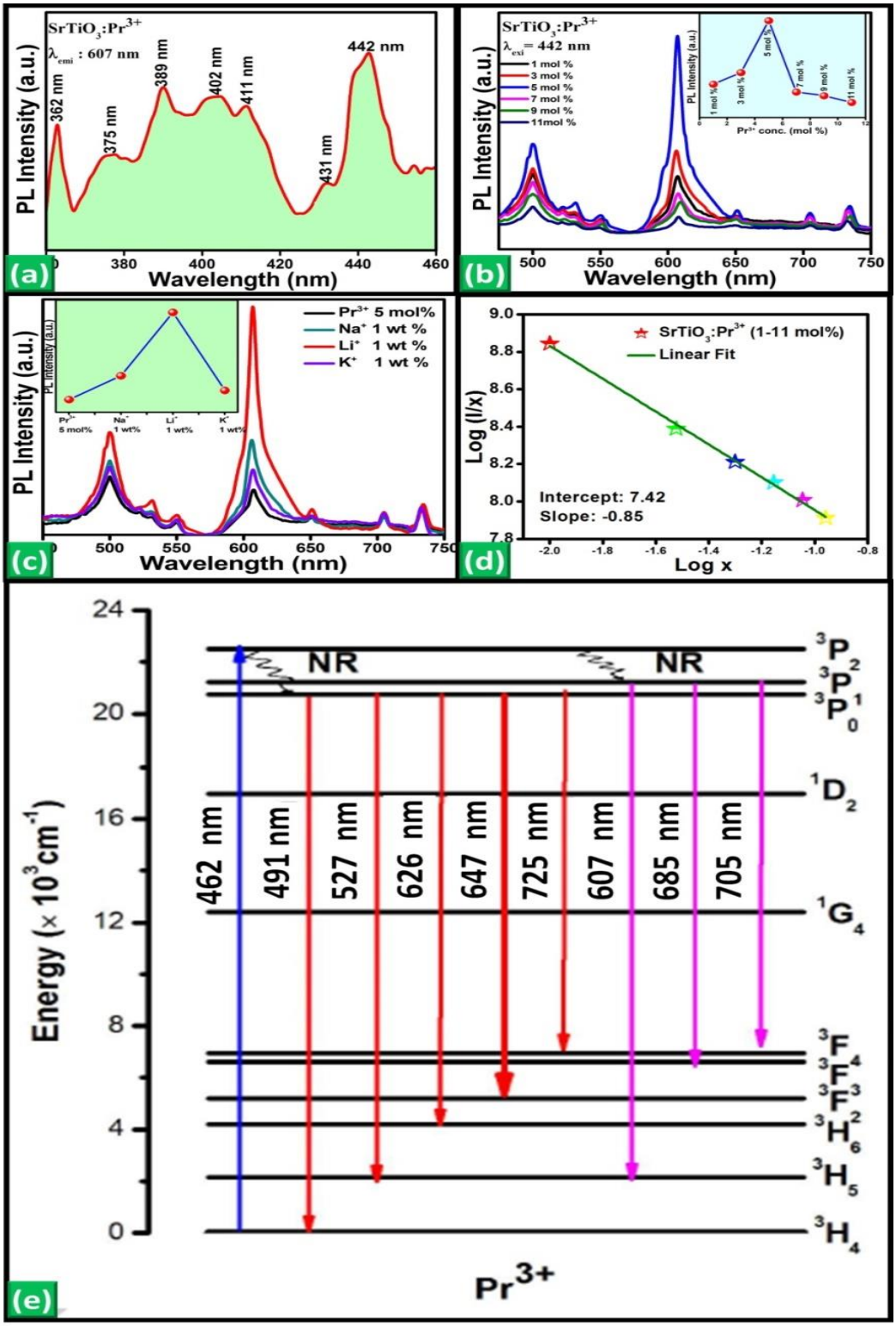

Fig.12 (a) PL excitation spectrum of $SriO_3$:Pr^{3+} (5 mol %) NPs under 607 nm emission. (b) PL emission spectra excited at 442 nm (c) Effect of monovalent ions on the PL intensity (d) shows the slope of log (I/x) versus log(x) (e) Energy level diagram of Pr^{3+} ions in $SrTiO_3$ host.

ACCEPTED MANUSCRIPT

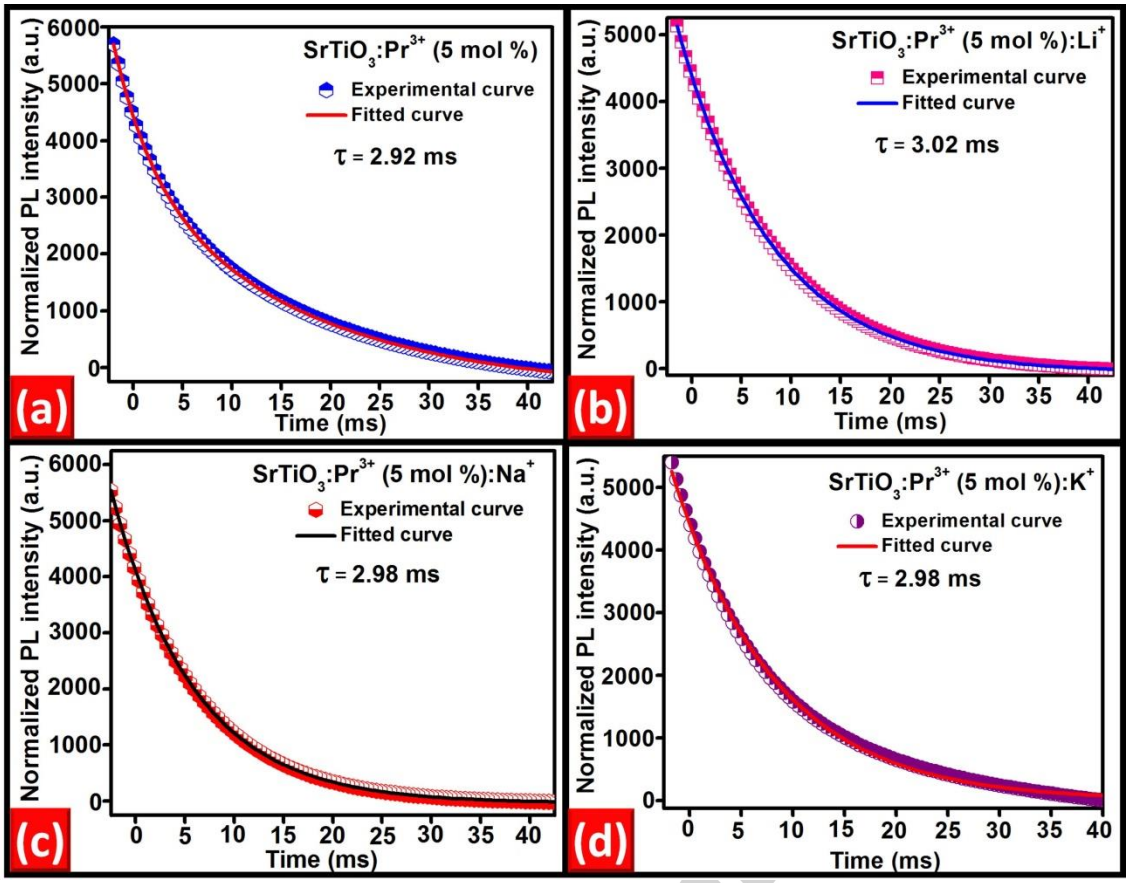

Fig.13 Decay curves of $SrTiO_3:Pr^{3+}$ (5 mol %), Na^+, K^+, Li^+ NPs under 442 nm excitation and 607 nm wavelength emission.

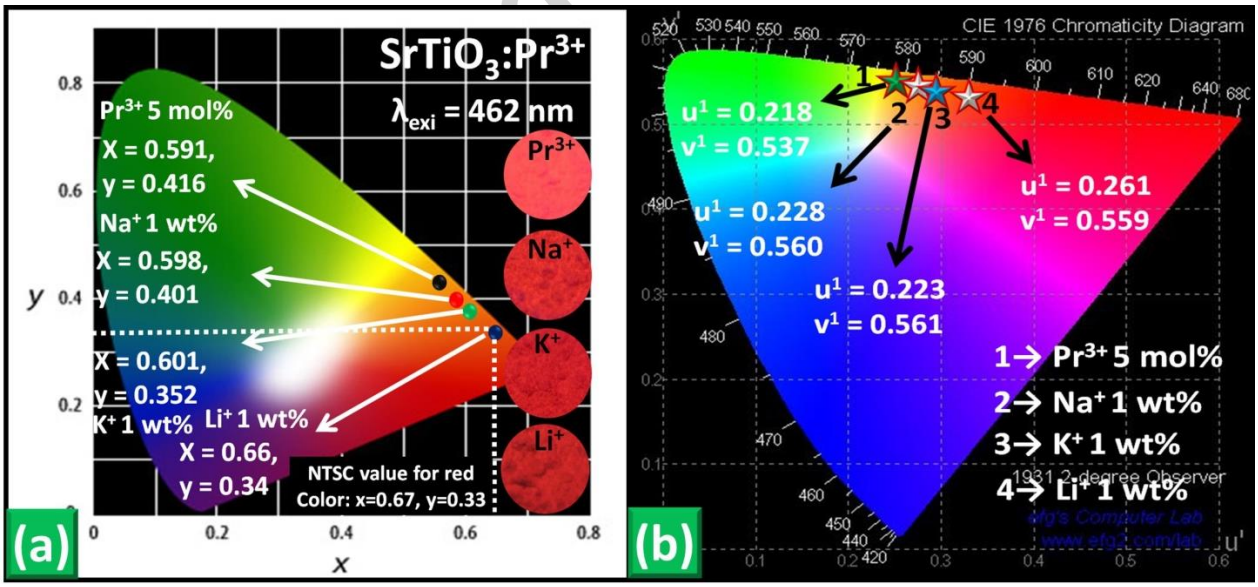

Fig.14 (a) CIE diagram and (b) CCT estimated values using the transformation equations.

ACCEPTED MANUSCRIPT

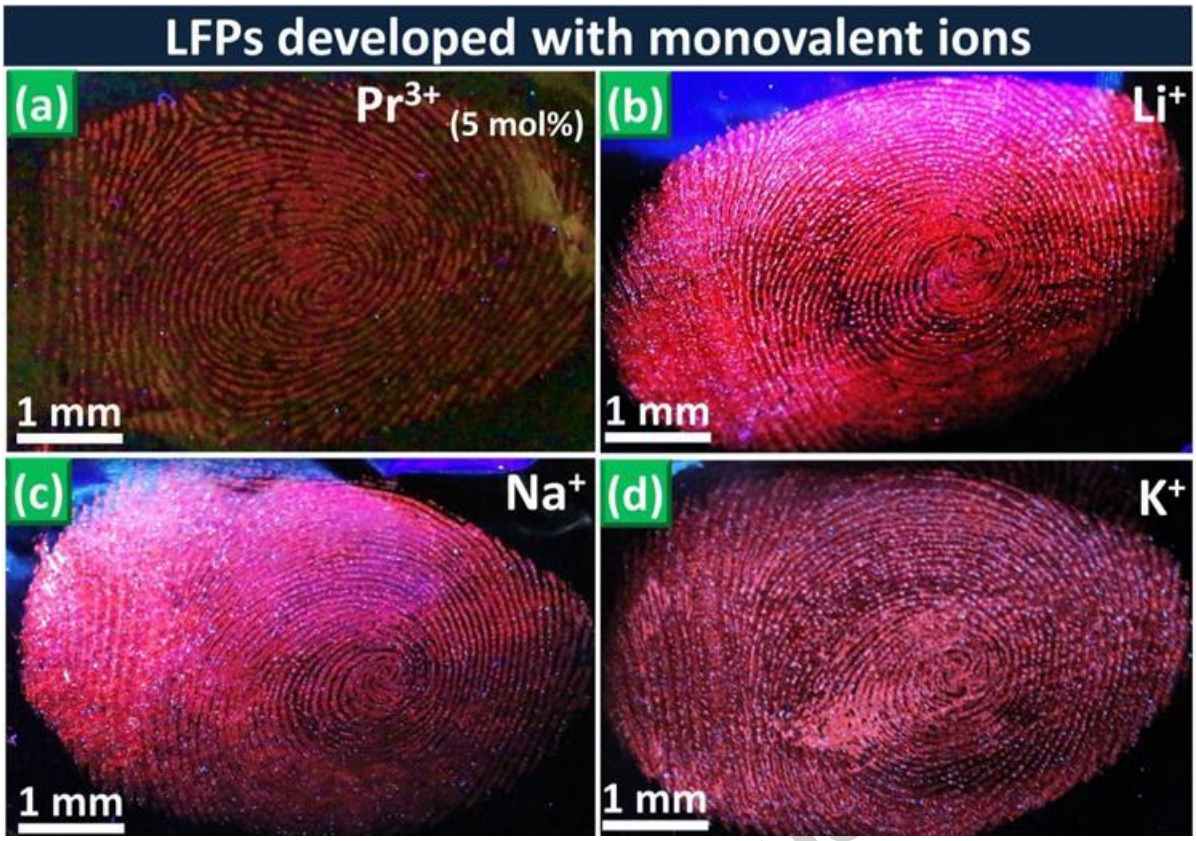

Fig.15 LFPs visualized with various monovalent metal ions (Na^+, K^+, Li^+) on aluminum foil surface.

Accepted manuscript

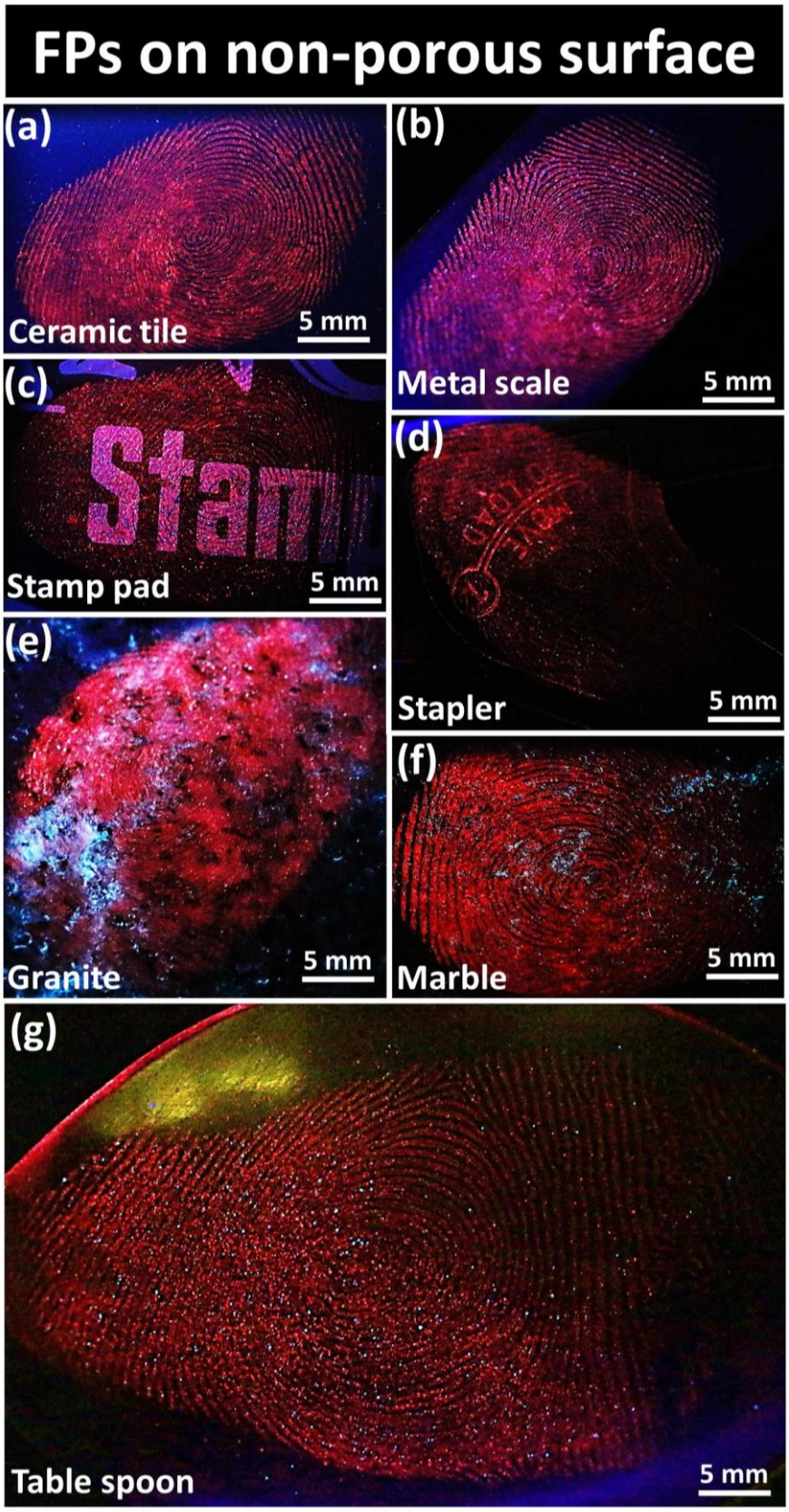

Fig.16. LFPs visualization on non-porous surfaces using $SrTiO_3:Pr^{3+}$ (5 mol %): Li^+ (1 wt%) NPs under 254 nm UV light.

ACCEPTED MANUSCRIPT

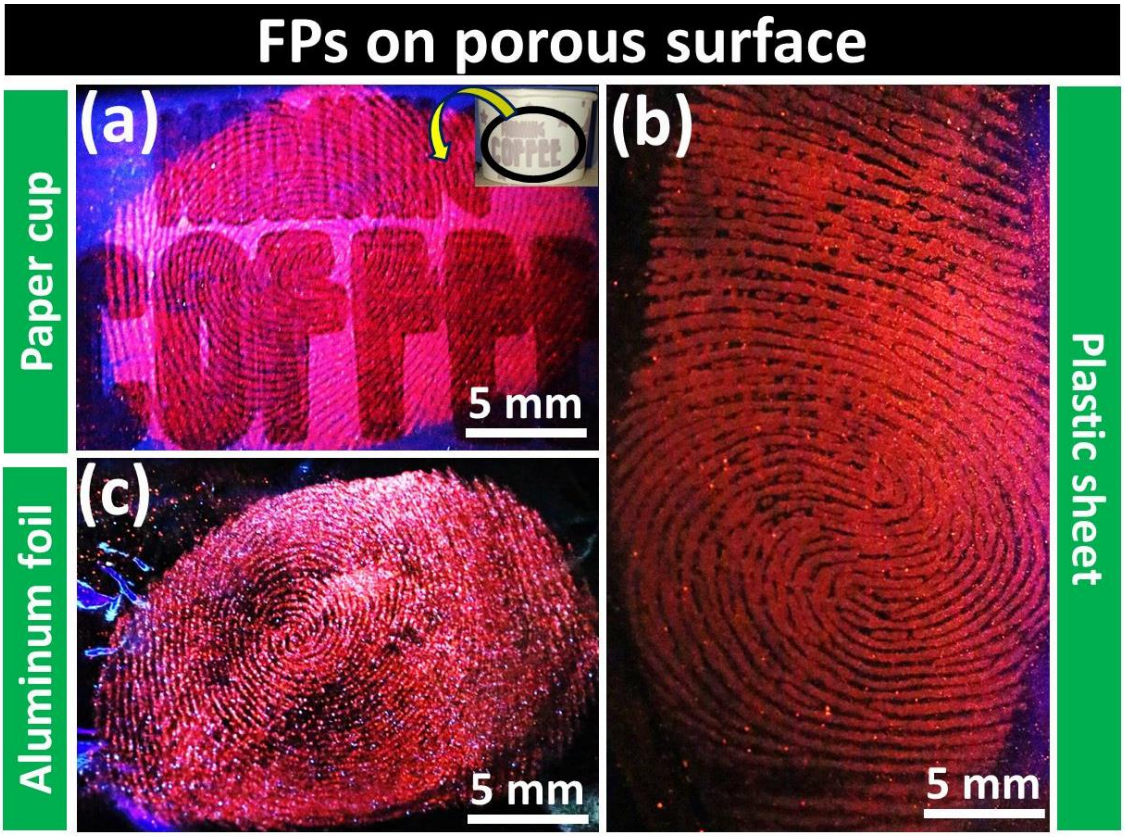

Fig.17. LFPs visualization on porous surfaces using $SrTiO_3:Pr^{3+}$ (5 mol %): Li^+ (1 wt%) NPs under 254 nm UV light.

Accepted manu

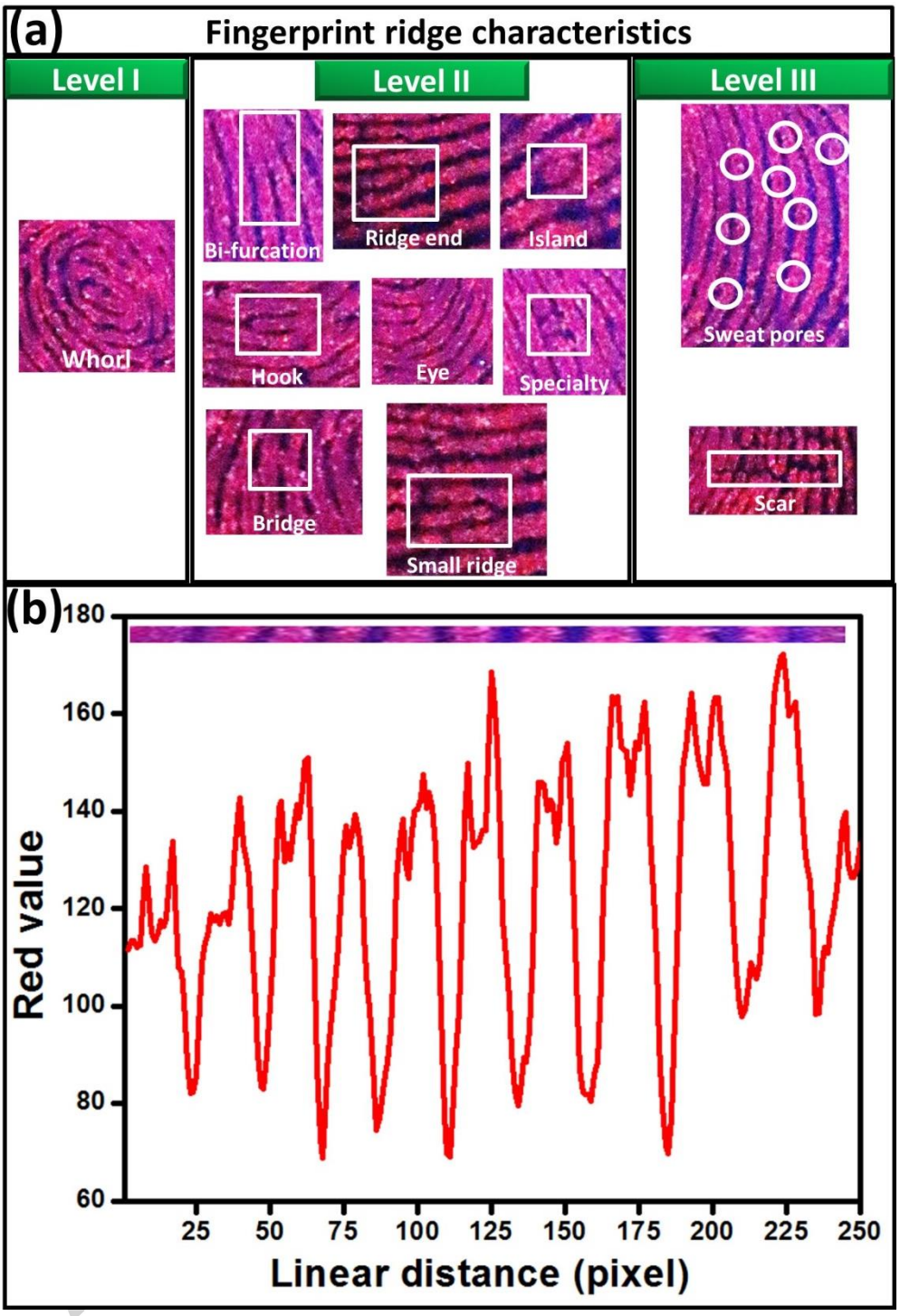

Fig.18. (a) Fingerprint ridge characteristics visualized on aluminum foil surface and (b) pixel profile image and (b) pixel profile showing the fluctuation of red value with ridge (red) and furrow (black) over a few papillary ridges indicated by rectangle box (Fig.18a).

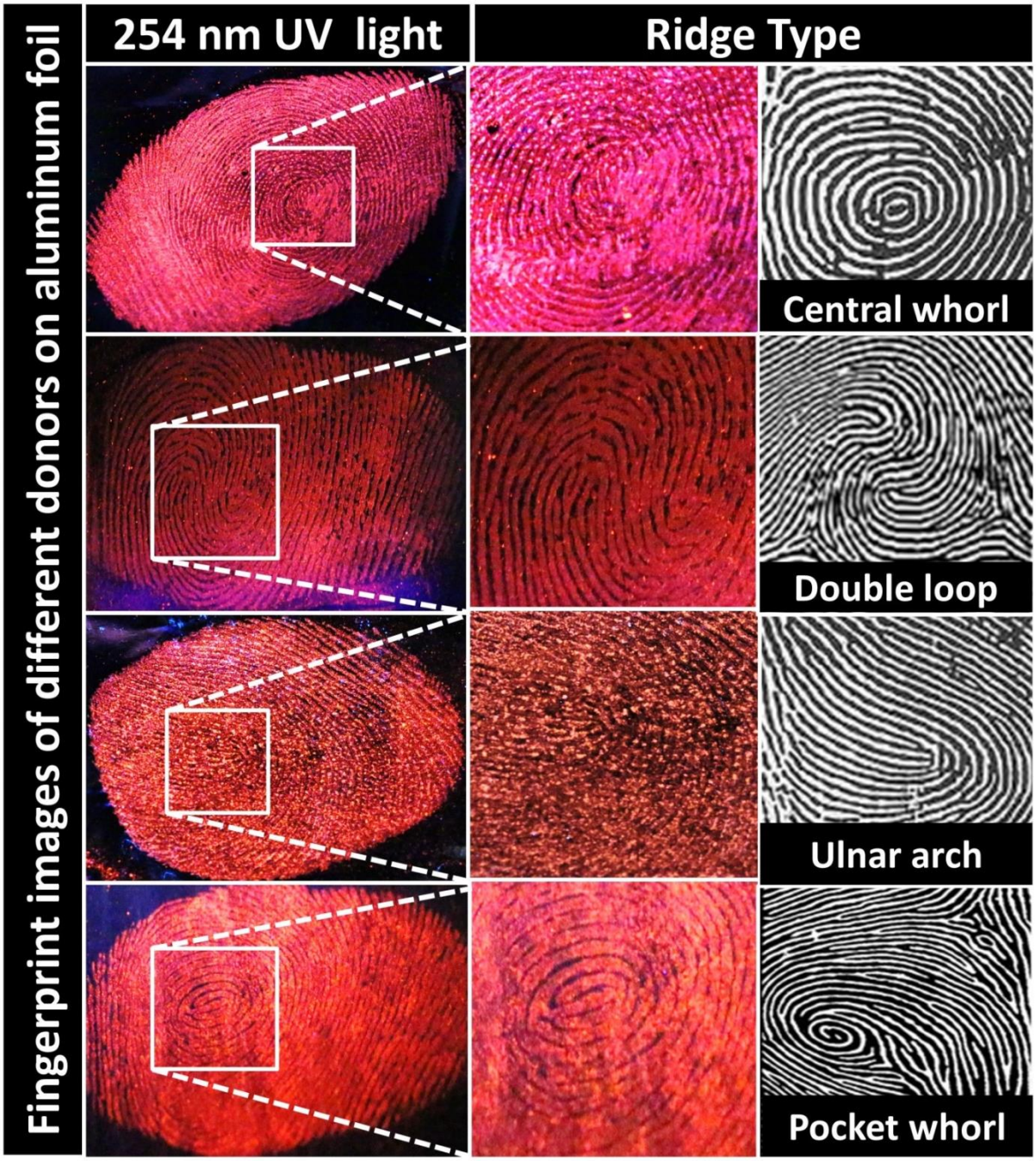

Fig.19. Visualization of LFPs type of various donors using $SrTiO_3$:Pr^{3+} (5 mol %): Li^+ (1 wt%) NPs on aluminum foil surface under 254 nm UV light.

ACCEPTED MANUSCRIPT

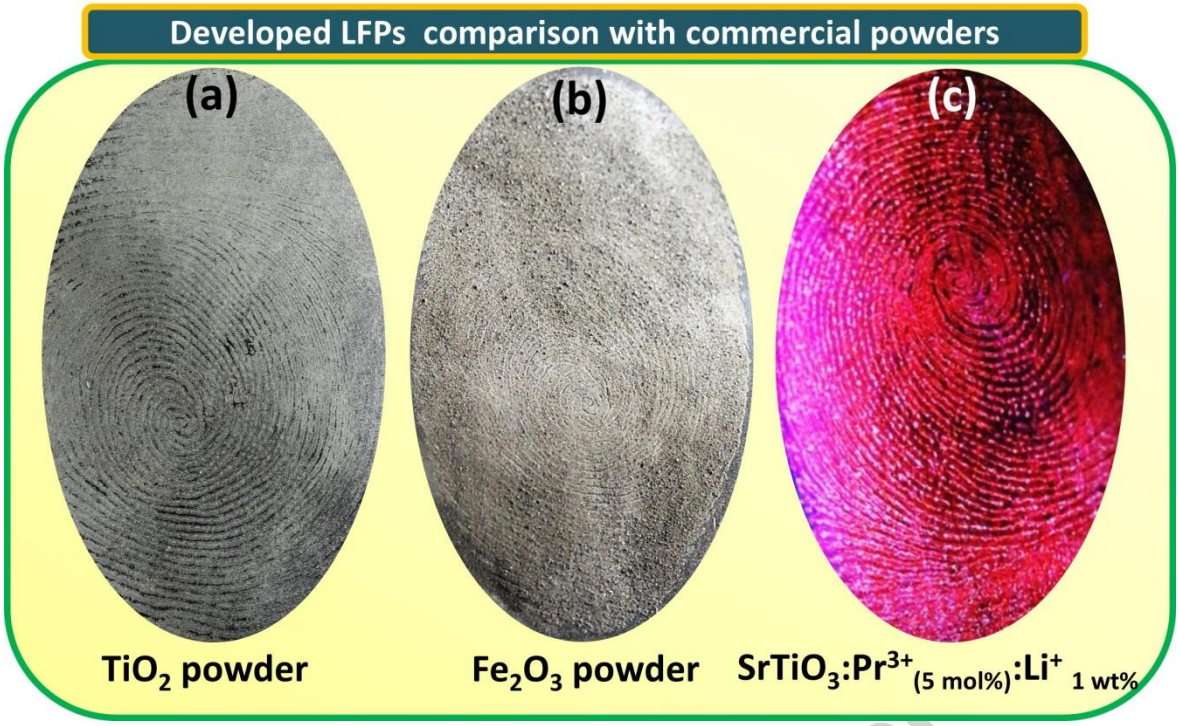

Fig.20. Comparison of LFPs visualized using $SrTiO_3:Pr^{3+}$ (5 mol %): Li^+ (1 wt %) with commercial powders.

Accepted manuscript

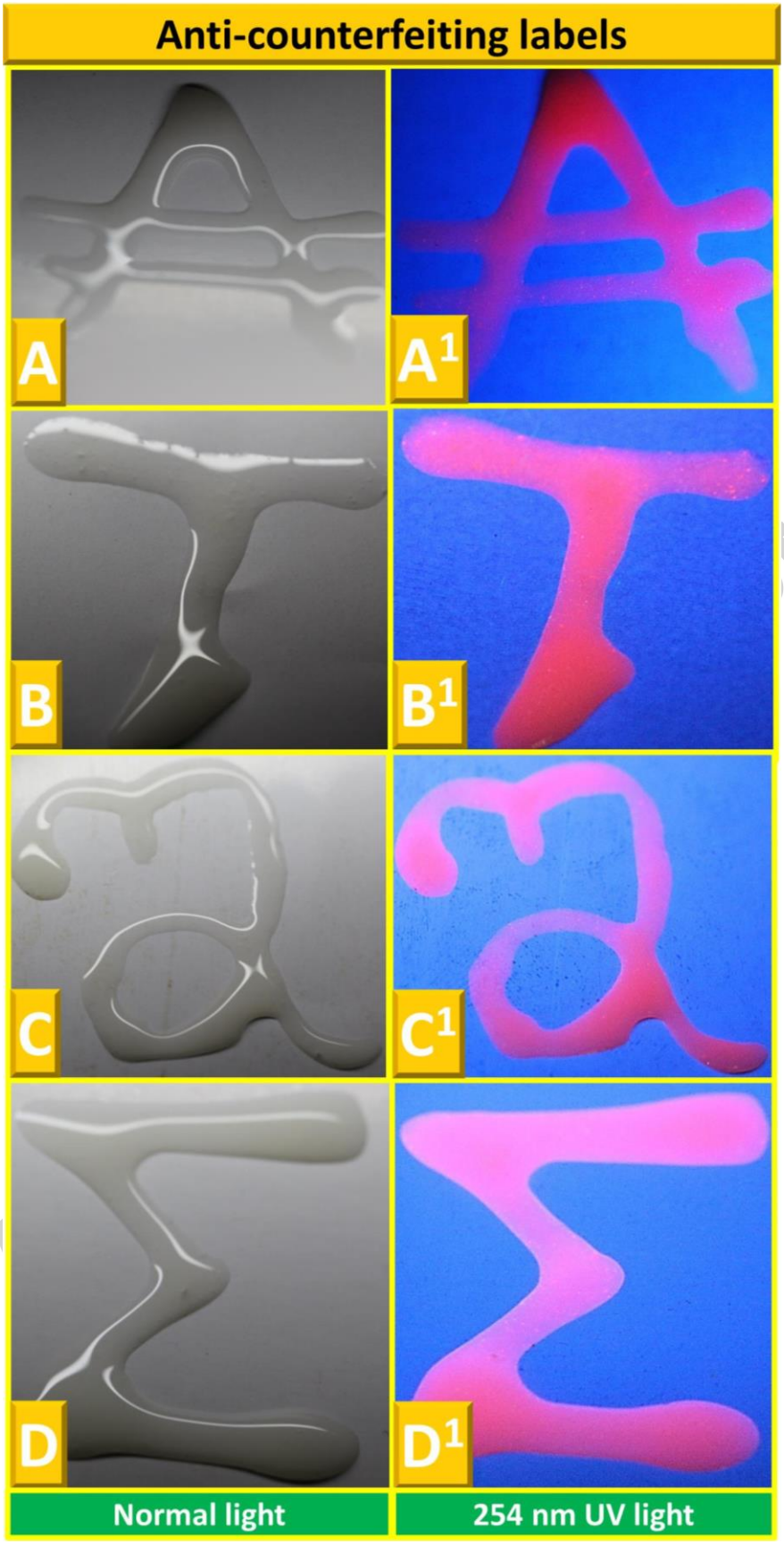

Fig.21. Anti-counterfeiting labels visualized under normal and 254 nm UV light.

ACCEPTED MANUSCRIPT

Table.1 The estimated average crystallite size and micro strain values of $SrTiO_3:Pr^{3+}$ (5 mol%) NPs with and without monovalent ions.

Monovalent ions (1 wt %)	Crystallite size (nm)		Micro strain x 10^{-3}
	Scherer's method	W-H plots	
No metal ion	23	30	2.89
Na^+	29	23	2.75
K^+	30	20	3.13
Li^+	33	21	3.40

Table.2 CIE chromaticity co-ordinates, CCT values, color purity and quantum efficiency of $SrTiO_3:Pr^{3+}$ (5 mol %) NPs with and without monovalent ions.

Sample	CIE		CCT		CCT values (K)	Color purity (%)	Quantum efficiency (%)
	x	y	u^1	v^1			
$SrTiO_3:Pr^{3+}$ (5 mol %)	0.591	0.416	0.218	0.537	1853	78	67
Na^+ (1 wt %)	0.598	0.401	0.228	0.560	1864	79	73
K^+ (1 wt %)	0.601	0.352	0.223	0.561	1804	82	76
Li^+ (1 wt %)	0.624	0.378	0.261	0.559	1862	85	78

Accepted manuscript